Title
Experimental determination of quartz solubility in KCl-H2O solutions at 7.5 and 10 kbar and 600-800°C

Author
Pempeña, Napoleon

Publication Date
2017

Peer reviewed|Thesis/dissertation

UNIVERSITY OF CALIFORNIA

Los Angeles

Experimental determination of quartz solubility in KCl-H_2O solutions at 7.5 and 10 kbar and 600-800°C

A thesis submitted in satisfaction of the requirements

for the Master's Degree in Geochemistry

by

Napoleon Pempeña VII

2017

ABSTRACT OF THE THESIS

Experimental determination of quartz solubility in KCl-H_2O solutions

at 7.5 and 10 kbar and 600-800°C

by Napoleon Pempeña VII

Master of Science in Geochemistry

University of California, Los Angeles, 2017

Professor Craig E. Manning, Chair

Brines are potentially important agents of mass transfer in the lower crust and subduction zones. Experiments and models typically assume that alkali-halide solutions can be approximated by the system NaCl-H_2O. However, KCl is also likely to be abundant in high pressure and temperature fluids, and the effect of this solute is unknown. We experimentally determined the solubility of quartz in H_2O-KCl solutions at 7.5 and 10 kbar and 600-800°C. We used hydrothermal piston cylinder methods and determined solubility by weight loss.

At 10 kbar and 800°C, quartz solubility is 1.23 mol SiO_2/kg H_2O in pure H_2O. Quartz solubility increases slightly with addition of a small amount of KCl up to 0.06 bulk KCl mole fraction (X_{KCl}). At higher X_{KCl}, quartz solubility decreases exponentially to 0.19 mol SiO_2/kg H_2O at sylvite saturation (X_{KCl} = 0.70). Quartz solubility decreases with T at constant X_{KCl}. At 700°C and 600°C, quartz solubility at sylvite saturation (X_{KCl} = 0.60 and 0.54, respectively) is

0.22 and 0.17 mol SiO_2/kg H_2O. At 7.5 kbar, "salting in" or silica solubility enhancement is observed at $X_{KCl} < 0.025$. Solubility then decreases monotonically.

Solubility variations at different P, T and salt types can be compared using the relative solubility (i.e., observed solubility divided by that in pure H_2O at P, T). In H_2O-NaCl solutions at 10 kbar, relative solubility decreases with rising NaCl mole fraction independent of temperature. This is not seen at high P in KCl-H_2O solutions. Relative quartz solubility measurements in KCl-H_2O solutions at 7.5 and 10 kbar are higher than in NaCl-H_2O solutions at any given salt mole fraction. Values in KCl-H_2O solutions are comparable to those in NaCl-H_2O solutions at lower P of ~5 kbar. This could be a result of the formation of hydrated KCl-SiO_2 complexes.

Textural and geochemical analyses of many petrologic examples indicate mass transport of silicates and mineral paragenesis enabled by alkali-rich, low-a_{H_2O} fluids. This newly discovered enhancement of silica solubility in KCl-H_2O solutions implies the possibility of significant silica metasomatism involving potassic salt solutions in deeper environments.

The thesis of Napoleon Pempeña VII is approved.

Edwin Arthur Schauble

Edward Donald Young

Craig E. Manning, Committee Chair

University of California, Los Angeles

2017

1. INTRODUCTION 1

2. METHODS 2

2.1. Starting materials 2

2.2. Capsule loading 3

2.3. Piston cylinder experiment 3

2.4. Quartz ball recovery 5

2.5. Weighing procedures 5

2.6. Post-run textural analysis 6

3. RESULTS 6

3.1. Run product textures 6

3.2. Uncertainty 7

3.3. Effects of X_{KCl}, temperature and pressure on solubility 9

4. DISCUSSION OF RESULTS 9

4.1. Sylvite saturation 9

4.2. Comparison with NaCl-H_2O solutions 10

4.3. Water activity model 11

4.4. Quartz solubility model 13

4.5. Silica hydration number 14

4.6. Formation of hybrid complexes 15

4.7. Petrologic applications 18

4.7.1. Granulite petrogenesis and migmatization 18

4.7.2. Fluid-assisted granite genesis 21

5. CONCLUSIONS 22

TABLES 24

FIGURES 27

REFERENCES 48

ACKNOWLEDGEMENTS

To Craig, thank you for your mentorship, trust and knowledge that you have shared. You have taught me to aim high and to work meticulously and confidently.

To Bob, thank you for your contagious enthusiasm in solving the esoteric and for lending your time even with the humblest of tasks. To the rest of PTXers Adam, Rosario, Daniel and Dan, thank you for your lending time and energy to help me gather my data and for lending a wrench, duct tape and your humor that made life in the lab enjoyable and memorable.

To the incredibly supportive faculty and staff of UCLA EPSS Department and Murphy Hall, thank you for going the extra mile to support your students. Thank you, Ed and Edwin for your feedback and enthusiasm to be part of my thesis committee.

To my family, friends, partner and my community outside academia, thank you for keeping me grounded and happy. You all contributed to my ability me to thrive in academia in the last two and a half years. It is because of all of you that I aspire to succeed in whatever I do.

It is with and for all of you that I will continue my pursuit of science discovery and education for the betterment of society.

1. INTRODUCTION

Dissolved silica is an important component of crustal fluids that can control the composition (Bebout and Barton, 1997), structure and rheology of the crust (Lund et al., 2006; Renard et al., 2000). Quantitative understanding of silica solubility is necessary to advance our knowledge of hydrothermal fluids and processes. The solubility of silica in pure water has been studied at various pressures (*P*) and temperatures (*T*) of geologic interest (Kennedy, 1950; Weill and Fyfe, 1964; Anderson and Burnham, 1965, 1967; Somerfeld, 1967; Crerar and Anderson, 1971; Manning, 1994). However natural fluids are complex. This has motivated many workers to study the effects of solutes such as NaCl, Ar, and CO_2 on quartz solubility over the past several decades.

H_2O-CO_2 solutions have been shown to decrease the solubility of quartz with increasing CO_2 concentration at fixed P and T (Shettel, 1974; Novgorodov, 1975; Walther and Orville, 1983; Newton and Manning, 2000, 2009). Meanwhile, quartz solubility in NaCl-H_2O solutions is more complex. At low to moderate P and high T, solubility increases as NaCl mole fraction (X_{NaCl}) increases up to a certain X_{NaCl} ('salts in') and then solubility declines monotonically or 'salts out'. At high P (10 kbar), quartz solubility declines exponentially with increasing X_{NaCl} (Newton and Manning, 2000; Shmulovich et al., 2006). CsCl-H_2O solutions show similar salting in and salting out behavior at all P and T investigated while CaCl-H_2O solutions show similar behavior only at high T and low P (800°C and 2 kbar; Shmulovich et al. 2006). Shmulovich et al. (2006) showed that at 800°C and 5 kbar, KCl-H_2O solutions achieve relatively higher quartz solubility than do NaCl-H_2O solutions at the same salt concentration.

Studies of solid inclusions found in metamorphic rocks from Campolungo and Adamello Complex, Italy (Ulmer 1983; Trommsdorff et al., 1985) and from the Alps (Scambellini and Philippot, 2001) indicate that sylvite and halite crystals could precipitate during prograde and retrograde metamorphism. For example, metamorphic reactions that consume H_2O could concentrate salts in the residual fluid (Trommsdorff et al., 1985). Our knowledge of the nature and occurrence of KCl brine as a metamorphic fluid is limited but geologic evidences suggest that it may be a powerful metasomatizing agent in lower crustal settings.

This study investigates quartz solubility in KCl-H_2O solutions at pressure and temperature regimes of the deep crust. A primary focus is on newly discovered enhancement of silica solubility in these solutions. The work provides a foundation to explore a new hypothesis for aqueous silica speciation for aqueous silica speciation in alkali-chloride solutions proposed by Evans (2007) and expanded on by Newton and Manning (2015). The new results establish that KCl-bearing deep crustal fluids may be important agents of metasomatism.

2. METHODS

2.1. Starting materials

Solubility experiments were conducted following methods used by Cruz and Manning (2015). Natural, high purity Brazilian quartz pieces were used. Quartz pieces were polished using a diamond file to nearly spherical shape. Fine polishing was done by rolling the balls successively on aluminum oxide sand paper with grit sizes 400, 600, 800 and 1200 (24, 14, 12, and 5 μm, respectively). Fine polishing generated uniform shape and surface morphology that minimize problems with crystals breaking and establish a baseline for post-run textural analysis. Quartz balls in runs with $X_{KCl} > 0.3$ were further polished to 1 μm since quartz ball surface

texture changes less in more concentrated solutions. Quartz balls must weigh between 1.6 - 3.2 mg as smaller quartz balls may completely dissolve or result in vanishingly small post-run mass while larger quartz balls tend to fracture during the run, giving anomalous post-run mass and solubility. After polishing, quartz balls were sonicated for several seconds and dried.

Distilled and deionized ~18 MΩ cm^3/cm H_2O was used in all experiments. We baked pure KCl at 300°C for at least 5 min. prior to loading to minimize adsorbed H_2O.

2.2. Capsule loading

Capsules were made from 3.5 mm OD Pt tubing with 0.18 mm wall thickness. Pt tubes were first cut into 1.27-1.54 cm segments, crimped and welded shut on one end and then annealed. Each charge was made by loading a capsule onto a weighing boat and components of desired calculated amounts were added into the capsule. Component mass was determined by mass difference using Mettler Toledo ultramicrobalance with $1\sigma = 0.2$ μg. Any excess H_2O added was evaporated until desired mass was achieved. The capsule was then crimped shut and the top was snipped off to prevent further H_2O loss. The capsule was then sealed using graphite arc welding. After welding, the capsule was weighed to determine mass loss from Pt vaporization. Capsules incurring significant mass loss after welding were discarded.

2.3. Piston cylinder experiment

Furnace assemblies consisted of NaCl, which plastically transmits pressure to the charge, with a graphite heater sleeve. The charge was situated at the vertical midpoint of the assembly with long axis of the charge being perpendicular to that of the assembly. A Pt shield was used to prevent the thermocouple from piercing the charge.

The cold, piston-out piston cylinder method was employed with a furnace design from Bohlen (1994) that requires no correction between the pressure experienced by the charge and that exerted by the piston. Temperature was measured using Pt-Pt_{90}Rh thermocouple with an accuracy of ±0.1°C, sheathed in mullite and MgO. Manning and Boettcher (1994) found that $\Delta T = 12.27 - 0.025T_{hot\ spot}$, with ΔT being the temperature difference between the hot spot and a spot 4 mm above the hot spot. Thus ΔT is ~8, ~5 and ~3°C at $T_{hot\ spot}$ of 800, 700 and 600°C, respectively. But realistic temperatures difference may even be smaller since temperature gradients are not linear (Ayers et al., 1992).

Experiments were conducted at 10 kbar and 800, 700 and 600°C; and at 7.5 kb and 800 and 600°C (Table 1). Pressure was brought up to 75% of the desired value. Temperature was then increased step-wise to the desired value. Thermal expansion compensated for the pressure deficit. Excess pressure was bled until equilibrium was achieved at ~6 hrs. Pressure was monitored using a bourdon tube Heise gauge with an accuracy of ±0.3 kbar. The maximum pressure deviation was 172 bars from desired pressure. The majority of experiments were run for 19-25 hours. All experiments were quenched by cutting power, which rapidly dropped temperature to ~100°C within ~2 mins.

Time series studies were conducted to verify the effects of vapor transport crystals (VTC; Caciagli and Manning, 2003; Antignano, 2008) for runs involving very dilute solutions ($X_{KCl} < 0.1$). Several charges of $X_{KCl} = 0.04$ were run for 1, 3, 6, and 19 hrs as well as charges of $X_{KCl} = 0.015$ for 1, 2, 3, 6, and 19 hrs.

2.4. Quartz ball recovery

Upon quenching, the capsule exterior was rinsed with distilled H_2O to remove adhering NaCl. The capsule was then dried and weighed. Capsules incurring significant mass loss were interpreted to have leaked and were discarded. After confirmation of negligible mass loss, the capsule was cut open and pH was measured. The pH remained constant at pH = 4 for 90% of the runs. Transparent, faceted, sylvite crystals precipitated in some capsules run with higher KCl concentrations and were preserved for analysis. Otherwise, the capsule was flushed with distilled H_2O. Recovered quartz crystals were sonicated to remove fine particles (up to 10 μm) stuck on the surface. However, some particles were still stuck after sonication, which were further removed by rolling the quartz balls between wet task wipes. Recovered quartz balls were then dried for final weighing.

2.5. Weighing procedures

Component mass was determined by mass difference using a Mettler Toledo ultramicrobalance with $1\sigma = 0.2$ μg. A plastic boat served as a weighing vessel during capsule loading while a smaller improvised Pt boat was used in weighing the post-run crystal for solubility measurements. Each weighing measurement was iterated 3 times. The average standard error (SE) in the measurement of the masses of the Pt, KCl granules and crystal is 0.75 μg and with a maximum SE of 1.61 μg. The average SE in the measurement of the mass of H_2O is 0.97 μg with a maximum SE of 1.97 μg. The higher standard error in H_2O weighing is due to its volatility. Attentiveness is crucial in ensuring H_2O does not touch the neck of the Pt capsule. Otherwise, H_2O will be squeezed out upon crimping and welding and will compromise the integrity of the capsule. The average SE in the measurement of the mass of the post-run crystal is

0.64 μg and with a maximum SE of 1.6 μg.

2.6. Post-run textural analysis

Back-scattered electron (BSE) imaging was used on selected post-run crystals to investigate the correlation of dissolution textures with the range of P, T and X_{KCl} conditions investigated. After the crystals were rinsed off and dried, they were examined for fractures using a binocular light microscope. Crystals free of observable fractures were then imaged using a Tescan Vega-3 XMU variable pressure scanning electron microscope (SEM) housed in UCLA's Ion Microprobe Facility. Each crystal was mounted on a 1 cm round aluminum mounts coated with carbon tape. Each crystal was then bombarded with an electron beam at 20.0 kV and a working distance of 21-28 mm under low vacuum.

Quench products and sylvite crystals from several runs were also imaged using the same SEM settings except that the working distance was 33-36 mm.

3. RESULTS

3.1. Run product textures

Dissolution during experiments modified the initial, nearly spherical quartz crystals through mass loss and mass redistribution; generally, the extent of modification was minor at high X_{KCl} and substantial at low X_{KCl} (Fig. 1). The concentration of KCl (X_{KCl}) is the primary variable and temperature is the secondary variable in the modification of quartz crystals up to the region of sylvite saturation (see discussion in Discussion of Results). Pressure has the least effect on modification in all conditions.

At low X_{KCl} (X_{KCl} =0.1-0.3 at 800°C and X_{KCl} <0.1 at 600°C), run product quartz crystals exhibit the greatest degree of modification (Fig. 1A) in the form of well-formed facets, dissolution grooves, craters and almost complete transformation into nearly euhedral hexagonal crystals with pronounced prismatic terminations.

An intermediate degree of quartz crystal modification is represented by the formation of concentric parallel grooves, unevenly flat surfaces and rounded edges and corners (Fig. 1B-1C). This occurred at intermediate values of X_{KCl} = 0.3-0.7 at 800°C and X_{KCl} =0.2-0.4 at 600°C.

Minimal modification is evident from a range of textures: from no detectable changes to the formation of a few isolated patches of parallel grooves and incipient facets. This mode of modification exists at X_{KCl} > 0.7 at 800°C and X_{KCl} > 0.4 at 600°C.

Upon quenching, capsules with concentrated solutions contained milky white fluid while capsules with dilute solutions contained translucent to colorless fluid. After evaporation, the residue was found to consist of sylvite precipitates (up to 500 μm; Fig. 2A) and colloidal silica roe (1-5 μm in diameter; Fig. 2B). Colloidal silica roe is representative of the silica-rich fluid in dilute solutions. Experiments at conditions of sylvite saturation yielded sylvite crystals up to 2.5 mm (Fig. 2C-2D). These large crystals could easily be observed and recovered upon opening the capsule, prior to evaporation of quench fluid.

3.2. Uncertainty

Time series studies were conducted to determine the time dependence of solubility. Runs were conducted for 1-26 h at three compositions: X_{KCl} = 0.015, 0.04, and 0.43 (Table 2). Figs. 3-5 show that there is no correlation of solubility with time. Notably, results from experiments

involving dilute solutions (X_{KCl} = 0.015, X_{KCl} = 0.04) exhibit a larger spread in measured solubility than in the more concentrated solution (X_{KCl} = 0.43). We attribute this larger uncertainty to the greater difficulty of loading capsule with very minute amounts of KCl, typically 1/8 of the amount of KCl used at X_{KCl} = 0.43 with the same nominal water content.

The time series data were used to characterize the uncertainty in solubility determinations at other concentrations. Figure 6 illustrates the variation in the standard deviation of the solubility determined at each KCl concentration. The two data points that determined the standard deviation of solubility in pure H_2O at 10 kbar and 800°C are from Manning (1994) and Newton and Manning (2010). For the purposes of assigning uncertainty to the rest of the solubility data set, we assumed that there are two concentration regimes which characteristic uncertainty ranges. The two regimes are described by

$$\sigma = -1.185X_{KCl} + 0.0758; 0.015 < X_{KCl} \leq 0.0524 \quad (1)$$

$$\sigma = 0.0137; 0 = X_{KCl} > 0.0524 \quad (2)$$

Using energy dispersive x-ray spectroscopy, we identified the bright white spots (high *Z*) on the crystal surface to be Fe and Cr contamination (Fig. 1), which probably came from the metal file used to polish the crystals. Their potential contribution to the mass change was assessed by making the conservative estimate that a quartz crystal surface is coated by Fe and Cr specks covering an area of 1000 μm^2 and 10 μm thick. In this case, the Fe and Cr mass would only contribute an additional 0.001 molal standard error to the lowest solubility measurement. An even smaller uncertainty contribution can be expected for solubility measurements of greater magnitude. Accordingly, we assume that any contribution of Fe and Cr surface contamination to the quartz solubility is below detection.

3.3. Effects of X_{KCl}, temperature and pressure on solubility

Figures 7-11 show the solubility data at 600-800°C and 7.5-10 kbar. At any given P and T, silica solubility in KCl-H_2O solutions decreases with increasing X_{KCl} up to sylvite saturation point. At both 10 and 7.5 kbar and constant X_{KCl}, solubility increases with increasing T. At 10 kbar and 800°C, solubility decreases only very slightly with increasing X_{KCl} up to $X_{KCl} \approx 0.12$, and then solubility drops rapidly up to saturation point, beyond which it remains constant (Fig. 7). At 7.5 kbar, there is apparent salting-in behavior described by an increase in solubility ($d\mathrm{m}(SiO_2)/dX_{KCl} > 0$) at $0 < X_{KCl} < 1$.

Pressure plays the least significant role in altering solubility. This is seen in the lack of significant difference in solubility between 10 and 7.5 kbar at 800°C and then again at 600°C.

4. DISCUSSION OF RESULTS

4.1. Sylvite saturation

Textural analysis of quench products and solubility measurements confirm theoretical predictions of sylvite saturation in KCl-H_2O solutions. Textural evidence (Figs. 2A-2D) varies as a function of X_{KCl} with the presence of large sylvite sylvite crystals coinciding with the theoretical sylvite saturation point (denoted in n Figs. 7-11). In addition, at any given P and T, solubility in the region $X_{KCl} \geq X_{KCl,sat}$ attains a constant value, indicating fixed fluid composition and sylvite crystallization during the run.

Aranovich and Newton (1997) derived theoretical sylvite saturation points from brucite-periclase-fluid equilibrium curves in the system KCl-MgO-H_2O by experimental reverse fluid

phase measurements and thermodynamic analysis. Experimental results from this study are consistent with the sylvite saturation conditions inferred by Aranovich and Newton (1997).

4.2. Comparison with NaCl-H_2O solutions

Solubilities in NaCl-H_2O versus KCl-H_2O solutions were compared across temperatures and pressures in terms of relative molality to be able to compare solubilities across P, T and salt species (Fig. 12). Relative molality of silica is defined in this study by solubility at a given X_{salt} normalized against m_0, the solubility of silica in pure H_2O at the same P and T. At 7.5 kbar and 800°C, the solubility of silica in pure H_2O is adapted from Manning (1994). Measurements beyond sylvite saturation point at each P and T are omitted in the comparison of relative molality.

All relative silica solubility data at 10 kbar at all temperatures fall along the same decreasing trend, regardless of temperature (Fig. 12). A similar trend can be observed for all data at 7.5 kbar but it persists to greater X_{KCl} than does the 10 kbar trend before decreasing more rapidly. Thus, within the investigated P-T range, relative molality in KCl-H_2O solutions is independent of temperature but slightly dependent on pressure. This is similar to the behavior found in NaCl-H_2O solutions by Newton and Manning (2010). However, KCl-H_2O solutions dissolve more SiO_2 than NaCl-H_2O solutions at a given P and T. For example, relative molality at 10 kbar in KCl-H_2O solutions is significantly higher than that in NaCl-H_2O solutions. Relative molality in KCl-H_2O solutions at 10 kbar is comparable to that in NaCl-H_2O solutions, which can achieve the same silica solubility at a little more than 4.35 kbar when extrapolated.

Relative molality in NaCl-H_2O solutions shows a change from simple monotonic decrease to a more complex trend as pressure decreases. This sudden salting in begins to occur

between 10 and 4.35 kbar in NaCl-H_2O solutions (Fig. 12). It is an enhancement in silica solubility described by an increase in relative molality up to a certain X_{KCl} and is then followed by a decrease. At 2 kbar, this enhancement persists up to 0.4 X_{KCl} before solubility returns to that in pure H_2O.

Salting in is also observed in KCl-H_2O solutions at 7.5 and 10 kbar. At 7.5 kbar, relative molality shows a slightly positive $d(m_{SiO2}/m_0)/dX_{KCl}$ along $X_{KCl} < 0.025$ until it plateaus and then it decreases gradually.

Although there is no increase in solubility relative to that in pure H_2O at 10 kbar, the concave downward trends exemplify the improvement in solubility achieved by KCl-H_2O solutions relative to NaCl-H_2O solutions at the same X_{salt} (Fig. 12). That is, the pivot of the $d(m_{SiO2}/m_0)/dX_{KCl}$ slope from steeply negative in NaCl-H_2O solutions to gradually negative in KCl-H_2O solutions shows relative improvement in silica solubility in KCl-H_2O solutions.

At $P < 7.5$ kbar, we expect a greater magnitude of salting in. In geologic settings, this means KCl-H_2O solutions can achieve similar silica solubility at greater depths than can NaCl-H_2O solutions (that is, $P_{KCl\text{-}H2O} > P_{NaCl\text{-}H2O}$ at fixed m_{SiO2}). Alternatively, KCl-H_2O solutions can achieve greater solubility than NaCl-H_2O solutions at the same depth (P) and X_{salt} (Fig. 12).

4.3. Water activity model

The influence of higher pressures and salinities on the thermodynamic behavior of aqueous KCl solutions is an important factor in understanding deep-earth metasomatic processes and understanding the activities of alkali chlorides and H2O is critical in making petrologic interpretations (Aranovich and Newton, 1997).

Aranovich and Newton (1996) measured H_2O and NaCl activities in concentrated NaCl-H_2O solutions in the range 2-15 kbar and 600-900°C by depression of the brucite-periclase equilibrium:

$$Mg(OH)_2 = MgO + H_2O \tag{3}$$

Because of physicochemical similarities between NaCl and KCl, pressure-induced changes in solute behavior can be expected for KCl (Aranovich and Newton, 1997). Thus for KCl-H_2O solutions we have a_{H_2O}:

$$a_{H_2O} = \frac{X_{H_2O}}{X_{H_2O}+(1+\alpha)X_{KCl}} \tag{4}$$

and a_{KCl}

$$a_{KCl} = \left[\frac{(1+\alpha)X_{KCl}}{X_{H_2O}+(1+\alpha)X_{KCl}}\right]^{(1+\alpha)} \tag{5}$$

implying H_2O and KCl mix ideally with variable degree of dissociation α, which depends on P and T but not on composition:

$$\alpha_{KCl} = \exp\left(4.166 - 2.709/\rho_{H_2O}\right) - 212.1P/T \tag{6}$$

where ρ is the density of H_2O in pure water at P and T in kbar and Kelvin, respectively. As pressure approaches 10 kbar, a_{H_2O} becomes approximately equal to the square of its molar concentration, X_{H_2O}. This is most probably due to the complete dissociation of KCl to K^+ and Cl^- : α approaches 1 as densities approach 1 g/cm^3. Here I use

$$a_{H_2O} = X_{H_2O}^2 \tag{7}$$

which Aranovich and Burnham (1997) have shown to hold between 4-15 kbar.

4.4. Quartz solubility model

A systematic understanding is necessary if we are to predict the effects of pressure, temperature and solute composition on quartz solubility and its implications in natural systems. One model was derived by Setchenow (1892) for quartz solubility from patterns seen in the interaction of organic compounds with salty fluids, which Schmulovich et al. (2006) modified to derive an empirical model to fit their experimental data. Their interpretation, however, does not ascribe the observed behavior to any physical model, and thus prevents extrapolation of solute behavior and quartz solubility outside the P-T range investigated.

Crerar and Anderson (1971) proposed a model to explain total saturation solubility of quartz in aqueous NaOH solutions in terms of solvated ionic and molecular species. Neglecting sodium-silica complexing, derived a solvation reaction for quartz:

$$SiO_{2(qtz)} + nH_2O = Si(OH)_4 \cdot (n-2)H_2O \quad (8)$$

which can be simplified to

$$SiO_{2(qtz)} + nH_2O = SiO_2 \cdot nH_2O \quad (9)$$

where $SiO_2 \cdot H_2O$ represents uncharged, solvated silica species with hydration number n. Walther and Orville (1983) assumes silica activity to be unity (Walther and Helgeson, 1977) to derive following equation for the reaction above:

$$\frac{d \log m_{SiO_2 \cdot nH_2O}}{d \log a_{H_2O}} = n \quad (10)$$

where $m_{SiO_2 \cdot nH_2O}$ is the molality of the dominant hydrated silica species and a_{H_2O} is the activity of H_2O. Various studies have found a range of values of *n* to be 4.4-5.3 from quartz solubility experiments at 2-5 kbar and 500-900°C in H_2O-CO_2 mixtures (Anderson and Burnham, 1965; Shettel, 1974; Novgorodov, 1975). Whereas analysis of quartz solubility data in and H_2O-CO_2 and Ar-H_2O mixtures find $n = 4$ (Walther and Orville, 1983). The wide uncertainty in these studies stem from the lack of H_2O-CO_2 mixing models to account for a_{H_2O} as well as from the lack of recognition of polymerization of aqueous silica at high P and T (e.g., Zotov and Keppler, 2002; Newton and Manning, 2002). Such deficits were addressed by Aranovich and Newton (1999), which derived thermodynamic mixing properties of in H_2O-CO_2 fluids to 15 kbar and 1000°C, and by Newton and Manning (2002, 2003), which experimentally contrained activity model for aqueous silica from 1-14 kbar and 600-900°C.

Evans (2007) formulated an expression for total dissolved silica in a SiO_2-NaCl-H_2O system incorporating proportions, dissociation parameters and activities of possible end member species among other factors. The stoichiometry of the dissolved silica species and the degree of salt dissociation are unknown parameters, which were calibrated by fitting the expression to prior experimental data on silica solubility. Overall, Evans (2007) used a model that accounts for pressure, temperature and salt concentration but neglects silica polymerization and assumes the alkali-silica complex to be anhydrous.

4.5. Silica hydration number

Hydration number *n* is one of the parameters tested by the Evans (2007) from *n*=1-4. She found that salting out is enhanced as *n* increases, i.e., solubility as a function of salinity shifts from having a sigmoidal trend to having a monotonically decreasing trend as *n* increases.

Figure 13 shows the comparison of values of hydration number *n* from studies of silica solubility in KCl-H_2O, NaCl-H_2O and CO_2-H_2O solutions (this study; Newton and Manning, 2000; Walther and Orville, 1983). A hydration number of 4 indicates that there are 2 H_2O molecules that are structurally part of the monomeric silica tetrahedron $Si(OH)_4 \cdot 2H_2O$ with 2 H_2O molecules hydrogen-bonded to the tetrahedron. NaCl-$H_2$0 solutions yield n=1.86, close to 2, indicating the existence of a monomer, $Si(OH)_4$, and a dimer, $Si_2(OH)_6$, without solvated H_2O. This implies that SiO_2 species in NaCl-H_2O solutions have negligible hydrogen-bonded H_2O of solvation at 800°C and 10 kbar. It also suggests that at high P and T, NaCl-H_2O solutions behave as if they were a solution of neutral atoms and molecules that inhibit the bonding of H_2O to silica (Newton and Manning 2006).

A smaller *n* of 1.26 for KCl-H_2O solutions then indicates greater suppression of silica solvation, implying that there is less H_2O participating in the formation of both monomers and dimers and yet KCl-H_2O solutions dissolve more silica than NaCl-H_2O solutions at a given P and T. This suggests that the solubility enhancement is due to the formation of a different silica species, possibly a hydrous SiO_2-KCl complex.

4.6. Formation of hybrid complexes

Newton and Manning (2009) combined high precision measurements of SiO_2 concentrations and activities of both H_2O and CO_2 to produce a simple model for quartz solubility in crustal H_2O-CO_2 fluids. Monomer in quartz-saturated solutions is produced by

$$SiO_{2(qtz)} + 4H_2O = Si(OH)_4 \cdot 2H_2O \qquad (11)$$

with an equilibrium constant:

$$K_{qm} = \frac{a_m}{a_{H_2O}^4} \tag{12}$$

where *q* and *m* denote quartz and monomer and *a* denotes activity. As silica increases, dimers are produced:

$$2Si(OH)_4 \cdot 2H_2O = Si_2O(OH)_6 \cdot 4H_2O + H_2O \tag{13}$$

with an equilibrium constant:

$$K_{md} = \frac{a_d a_{H_2O}}{a_m^2} \tag{14}$$

where *d* denotes dimer. Newton and Manning (2002, 2003, 2010) showed that the activities of the monomer and dimer can be consistently replaced by their mole fractions, leading to K_{md} being

$$K_{md} = 1.480 + 0.0012T + (0.000119T - 0.1685)P \tag{15}$$

where T is in Kelvin and P is in kbar.

Newton and Manning (2006) incorporated pressure-induced ionization, SiO_2 polymerization, and H_2O activity measurements of Aranovich and Newton (1996) to describe the relation of silica dissolution and NaCl dissociation. We adapt this for KCl on the basis of the physicochemical similarities between NaCl and KCl found by Anderson and Burnham (1997). Effectively, the silica dissolution and KCl dissociation are related by:

$$X_{SiO_2} = \frac{m_{SiO_2}}{m_{SiO_2} + 55.51\left[1 + \frac{(1+\alpha)X_{KCl}}{X_{H_2O}}\right]} \tag{16}$$

Newton and Manning (2015) postulated that the enhancement in quartz solubility at elevated T and P in NaCl- H_2O solutions is due to the complexing of silica with the solvent components. Following Evans (2007), the complexes are formed by

$$SiO_2 + xKCl + yH_2O = n \text{ solute complexes} \quad (17)$$

This general type of reaction has been used in modeling solubility of different minerals in NaCl-H_2O solutions at elevated T and P (Newton and Manning, 2010).

Assuming that the ideal solution relation for silica polymers holds for the hybrid complexes, the equilibrium constant K_{hc} for the above reaction is:

$$K_{hc} = \frac{X_{hc}^n}{a_{KCl}^x a_{H_2O}^y} \quad (18)$$

The total silica is defined by:

$$X_{SiO_2} = X_{hc} + X_m + 2X_d \quad (19)$$

where X_{SiO_2} is the total molar silica concentration, X_{hc} is the concentration of silica involved in the hybrid complex (regardless of the stoichiometric number of Si it contains) and X_m and X_d are respective monomer and dimer concentrations. Note that equation neglects higher Si polymers (trimers, etc.). Such species have not been observed in the P-T range of this investigation.

Figures 14-18 show the molar abundance of silica in the hybrid complex (X_{hc}) as a function of X_{KCl}. This behavior is similar to that found by Newton and Manning (2015) in NaCl-H_2O solutions. The trend of sharp increase in X_{hc} followed by monotonic decrease is seen at all conditions of this study. X_{hc} peak occurs within the range of X_{KCl}=0.12-0.2 but X_{hc} peak values

decrease strongly as function of T and only very slightly as a function of P. At 10 kbar, 800°C, X_{hc} increases very sharply until it peaks at about X_{KCl} =0.12 (Fig. 14). It then decreases monotonically. At 7.5 kbar, 800°C X_{hc} arguably peaks at about the same X_{KCl} but at a lower X_{hc} (Fig. 17).

Based on the assumptions and calculations above, monomers are the predominant form of dissolved silica alongside significant amount of dimers in pure water at 800°C and 10 kbar (Fig. 19). As X_{KCl} increases, monomer and dimer concentrations significantly decrease and hybrid complexes start to form and reach maximum abundance at X_{KCl} =0.12. At X_{KCl} =0.04, the hybrid complex overtakes as the dominant silica species until KCl saturation.

4.7. Petrologic applications

Various experimental and field studies increasingly highlight the importance of saline fluids in many petrologic phenomena. They not only provide explanations to previously unexplained phenomena but they also encourage reassessment of previously established models of some geologic processes.

4.7.1. Granulite petrogenesis and migmatization

Granulite facies assemblages and migmatites are important features of metamorphic terranes and anatexis provides a link to both (Hansen and Stuk, 1993). Anatexis could occur in an open or a closed system. Olsen (1985) and Powell (1983) suggested that in a closed system, internal buffering of a_{H_2O} would lead to the formation of granulite facies rocks by dehydration melting in which H_2O-bearing minerals react to form a melt and anhydrous solids. On the other

hand, Pattison (1991) argued for an open system model that combines anatexis with Si- and Na-bearing, low-a_{H_2O} fluids.

Hansen and Stuk (1993) studied orthopyroxene-bearing migmatites from Cone Peak, central California and interpret them to be products of partial melting in an open system. The typical host rock consists of a network of hornblende and biotite which encloses plagioclase and quartz. Orthopyroxene and clinopyroxene occur together in irregular patches sometimes connected to form irregular anastomosing veins. Hansen and Stuk (1993) argue that partial melting was triggered by an influx of K- and Si-bearing fluid that removed Ca and possibly Fe. This consumed hornblende to produce orthopyroxene in dehydration melting reactions (Fig. 20). Under conditions typical of high-grade metamorphism, melts and orthopyroxene are in equilibrium only at relatively low a_{H_2O}(Waters, 1988; Pattison, 1991).

Another assemblage exemplifying low-a_{H_2O} petrogenesis is found in the garnetiferous charnockitic rocks found in the southern extent of the Late Archean Dharwar Craton in the highlands of Krishnagiri, Tamil Nadu, India. Characteristically irregular K-feldspar mottling is found within plagioclase grains with a concentration at boundaries with orthopyroxene, garnet and rare biotite (Fig. 21). Plagioclase grains containing aligned K-feldspar in their interiors resemble anti-perthite exsolution lamellae but this is unlikely because of the irregularity of distribution and amount (Hansen et al., 1995).

Plagioclase grains situated next to either K-feldspar veinlets or quartz frequently show an increase of anorthite and a decrease of albite towards the margins. Orthopyroxene is unusually magnesian for felsic granulites (Mg/Mg+Fe=0.6-0.7) with an observable decrease of Al towards the margin. K-feldspar veins are relatively low in Na (about 6 mol % Ab) and very high in Ba

(0.5-2.5 wt. % BaO). Garnets are invariably zoned, with an increase of Ca towards the rims and a slight decrease of Mg and Fe. This observation is independent of proximity of garnets with K-feldspar-quartz veins.

The extreme dryness of the samples is manifest in the near-absence of hydrous minerals in felsic assemblages. Thus the inferred P, T conditions require that the charnockites with the assemblage orthopyroxene-K-feldspar-bitotite-quartz must have formed at $a_{H_2O} < 0.2$ based on phlogopite-quartz stability by Vielzeuf and Clemens (1992) up to a maximum of $a_{H_2O} = 3$ according to a model by Bohlen et al. (1983).

Perchuk and Gerya (1992, 1993) studied K-feldspar microvein networks in Eurasian charnockites, proposing that a very mobile grain boundary fluid could enable alkali ion mobilization. The ion-exchange reaction involved would be:

$$K^+ + NaAlSi_3O_8 = KAlSi_3O_8 + Na^+ \quad (20)$$

This is exemplified by plagioclase zoning in the Dharwar Craton charnockite where plagioclase crystals in contact with K-feldspar veins are more calcic and less sodic due to the removal of Na^+. Hansen et al. (1995) use this evidence to argue that the K-feldspar veins could not have crystallized from a granitic melt since this would require plagioclase crystals to have normal zoning, that is, having Na enrichment toward grain boundaries. Further, they attribute the decrease of Al in orthopyroxene towards the boundary as result of the introduction of K_2O from metasomatic fluids:

$$(Mg,Fe)Al_2SiO_6 + K_2O + 6SiO_2 = 2KAlSi_3O_8 + (Mg,Fe)SiO_3 \quad (21)$$

However, the decrease in Al in orthopyroxene rims may also be in part due to decreased temperature during late vein formation.

Using chemical analysis data and P-T estimates of 7.5 kbar and 800°C from Hansen et al. (1995), and using the hybrid silica species model proposed in this study, we calculate that the grain boundary fluids would have contained 0.22-0.26 X_{KCl}, dissolving roughly 0.74-0.85 mol SiO_2/kg H_2O. This is a 3.5-fold increase compared to the solubility if the dissolved silica only comprised monomers and dimers.

In conclusion, Hansen et al. (1995) attribute the formation of the K-feldspar vein network, atypical orthopyroxene formation in dry felsic granite, and the abovementioned mineral grain zonation trends to a pervasive grain boundary fluid with low viscosity and low a_{H_2O}.

Comparable microveining of granulites has been found by Coolen (1980) in Furua, Tanzania Complex; by Perchuk and Gerya (1992, 1993) in Siberian and Finnish charnockites; by Todd and Evans (1994) in Alaskan granulites; and by Sen (1959) in South Indian granulites, who called it "replacement antiperthite.

4.7.2. Fluid-assisted granite genesis

The prevailing thought about granite genesis and crustal evolution is that fluid-absent dehydration melting in a closed system enables crustal differentiation by upward removal of a granitic melt while leaving behind a volatile- and LILE-depleted granulite facies lower crust. Despite its successes, the theory remains inadequate in bridging key aspects of granite genesis and granulite-facies metamorphism. Some discrepancies observed are: (1) the insufficiency of known heat sources to generate observed granite masses supposedly produced solely by

dehydration melting; (2) the lack of sufficient H_2O in the protolith to yield required granitic melt volumes; (3) the inconsistent relations of observations in exposed terranes with LILE partitioning between granitic liquid and granulite residues; (4) the incompatibility of observed granulite grade migmatites with predicted leucosome compositions (Aranovich et al., 2014).

Aranovich et al. (2014) support an open system model of granite genesis involving volatile-rich, mantle-derived magma intruding into the deep crust. According to studies, this view is more consistent with observations of the uppermost subcontinental mantle being subjected to metasomatic processes (Stolz and Davies, 1989; Woolley, 1989; Barker, 1996). This model could provide the source of heat for large scale melting being the latent heat of crystallization of basalt. Volatile components could be incorporated into metasomatizing fluids that lower H_2O activity (Johnson 1991). If the fluids could advect heat (Ganguly et al., 1995; Bachmann and Bergantz, 2006), alkalis and halides, they could promote mid-crustal migmatization. The saline fluid component would be capable much more of intimate penetration of grain boundaries of rocks whan would a viscous silicate melt, hence, the microtextures observed in many granulites as described above. Further, localization of partial melting in the mid-crust may be explainable by the positive *dP/dT* slope achieved by saline solutions that lower water activity (Aranovich et al., 2013).

5. CONCLUSIONS

We conclude in this study that at 7.5 and 10 kbar and 600-800°C,

- Silica solubility in KCl-H_2O solutions decreases with increasing X_{KCl} except at 7.5 kbar at $X_{KCl} < 0.025$ where salting in occurs.

- Relative silica solubility in KCl-H_2O solutions is temperature independent and pressure dependent; and the transition from the absence to the presence of salting in phenomenon occurs between 7.5 and 10 kbar in KCl-H_2O solutions.
- KCl-H_2O solutions dissolve SiO_2 more effectively than do NaCl-H_2O solutions at a given P and T.
- KCl-H_2O solutions achieve a lower hydration than do NaCl-H_2O and CO_2-H_2O solutions, implying lower concentrations of monomers and dimers than in NaCl-H_2O and CO_2-H_2O solutions at a given P and T.
- KCl-H_2O solutions achieve enhancement in silica solubility while producing lower concentrations of hydrated silica species, indicating the potential existence of a hydrated KCl-SiO_2 complex as a silica species.

The ability of KCl-H_2O solutions to enhance silica solubility due to the existence of a hydrated KCl-SiO_2 complex as a dissolved silica species could explain various petrologic processes such as widespread deep crustal metasomatism and midcrustal granite genesis.

TABLES

Expt. No.	P (kbar)	T (°C)	time (hrs)	Initial qtz wt. (mg)	Final qtz wt. (mg)	H_2O wt. (mg)	KCl wt. (mg)	X_{H2O}	a_{H2O}	X_{KCl}	10^3* X_{SiO2}	m_{SiO2} (mol SiO_2/ kg H_2O)
QS1	10	800	6	2.380	0.476	25.749	0	1	1	0	21.690	1.231
QS67*	10	800						0.985	0.970	0.015	21.274	1.244
QS68*	10	800						0.960	0.921	0.040	19.593	1.203
QS10	10	800	24	2.373	0.768	22.595	7.691	0.924	0.854	0.076	17.955	1.182
QS2	10	800	18	1.615	0.259	20.841	11.196	0.885	0.783	0.115	15.251	1.083
QS3	10	800	25	3.026	1.603	26.232	27.139	0.800	0.640	0.200	10.733	0.903
QS4	10	800	24	2.398	1.533	19.996	35.538	0.700	0.489	0.300	6.925	0.720
QS69*	10	800						0.575	0.330	0.425	3.900	0.539
QS28	10	800	26	1.241	1.105	6.686	40.524	0.406	0.165	0.594	1.555	0.340
QS6	10	800	23	1.811	1.727	5.951	56.275	0.304	0.093	0.696	0.764	0.237
QS7	10	800	17	2.999	2.981	1.593	60.758	0.098	0.010	0.902	0.175	0.188
QS14	10	700	23	2.642	1.501	26.685	0.000	1	1	0	12.659	0.712
QS16	10	700	21	2.798	1.766	25.029	2.316	0.978	0.957	0.022	11.698	0.686
QS15	10	700	24.5	2.582	1.725	21.482	4.898	0.948	0.898	0.052	10.661	0.664
QS17	10	700	25	2.750	1.929	24.531	13.050	0.886	0.785	0.114	7.917	0.557
QS18	10	700	23	1.851	1.071	25.163	25.963	0.800	0.641	0.200	6.160	0.516
QS19	10	700	26.5	1.574	1.398	8.499	23.262	0.602	0.362	0.398	2.666	0.345
QS29	10	700	25.5	1.606	1.440	9.538	39.719	0.498	0.248	0.502	1.728	0.289
QS22	10	700	24.5	2.452	2.365	6.543	41.037	0.398	0.158	0.602	0.997	0.223
QS21	10	700	19	2.599	2.542	4.473	49.012	0.274	0.075	0.726	0.600	0.210
QS23	10	700	27	1.656	1.616	3.045	50.501	0.200	0.040	0.800	0.441	0.221
QS27	10	600	20.5	2.356	1.816	24.149	0.000	1	1	0	6.662	0.372
QS34	10	600	23.5	1.730	1.347	18.062	1.572	0.979	0.959	0.021	6.072	0.353
QS35	10	600	22	1.690	1.290	18.973	2.829	0.965	0.932	0.035	5.862	0.351
QS33	10	600	27	2.397	1.979	20.001	4.593	0.947	0.898	0.053	5.600	0.347
QS31	10	600	24	1.956	1.552	20.074	4.593	0.891	0.795	0.109	4.831	0.335

QS32	10	600	25	1.930	1.574	20.028	19.951	0.806	0.650	0.194	3.585	0.296
QS24	10	600	26.5	2.564	2.412	11.818	25.258	0.659	0.435	0.341	1.891	0.214
QS26	10	600	22.5	1.825	1.723	8.625	25.159	0.587	0.344	0.413	1.476	0.198
QS25	10	800	24	2.480	2.399	8.107	39.355	0.460	0.212	0.540	0.893	0.166
M94	7.5	800						1	1	0	18.226	1.031
QS59	7.5	800	19	2.023	1.085	14.187	3.123	0.949	0.902	0.051	17.600	1.100
QS50	7.5	800	25.5	2.695	1.741	18.363	15.000	0.835	0.697	0.165	11.043	0.865
QS51	7.5	800	22	2.237	1.409	19.724	33.268	0.710	0.505	0.290	6.887	0.699
QS57	7.5	800	21	2.467	2.408	4.580	44.035	0.301	0.091	0.699	0.689	0.216
QS55	7.5	800	21	2.521	2.492	2.601	39.873	0.213	0.045	0.787	0.399	0.186
QS52	7.5	600	22	2.635	2.098	28.960	0.000	1	1	0	5.530	0.309
QS58	7.5	600	23	2.071	1.795	13.921	3.203	0.947	0.897	0.053	5.327	0.330
QS53	7.5	600	22	2.484	2.224	18.039	33.063	0.693	0.480	0.307	2.282	0.239
QS56	7.5	600	22	2.028	1.948	8.203	33.493	0.503	0.253	0.497	0.975	0.161
QS60	7.5	600	24	1.962	1.924	3.927	17.834	0.477	0.227	0.523	0.906	0.161

Table 1. Conditions and measurements used to calculate quartz solubility. Experiment numbers marked with * show average X_{H2O}, a_{H2O}, X_{KCl} and 10^3*X_{SiO2} and m_{SiO2} of multiple data points. Full tabulation of time, initial quartz weight, final quartz weight, and KCl weight of experiments marked with * are shown in Table 2.

Expt. No.	time (hrs)	Initial qtz wt. (mg)	Final qtz wt. (mg)	H_2O wt. (mg)	KCl wt. (mg)	X_{KCl}	m_{SiO2} (mol/kg_{H2O})
QS13	23	2.303	1.628	20.418	1.297	0.015	1.327
QS36	1	1.521	1.214	15.536	0.986	0.015	1.300
QS37	2	1.900	1.080	15.587	0.994	0.015	1.153
QS38	3	1.211	1.128	15.614	0.994	0.015	1.202
QS39	6	2.030	1.117	15.039	0.953	0.015	1.236
QS11	19	2.190	1.758	23.039	4.018	0.040	1.270
QS40	1	2.663	1.493	20.536	3.586	0.040	1.210
QS41	3	2.015	1.513	20.417	3.557	0.040	1.233
QS42	6	1.612	1.086	14.905	2.588	0.040	1.213
QS45	3	1.717	1.306	17.922	3.147	0.041	1.213
QS43	3	2.321	1.290	18.318	3.182	0.040	1.172
QS44	3	2.482	1.315	18.414	3.207	0.040	1.188
QS46	3	2.032	1.281	17.992	3.121	0.040	1.185
QS47	19	2.073	1.313	18.241	3.153	0.040	1.198
QS49	19	2.719	1.269	18.449	3.238	0.041	1.145
QS5	26	3.037	0.228	7.203	22.299	0.428	0.526
QS61	26	1.631	0.252	7.893	24.074	0.424	0.530
QS63	26	2.154	0.265	8.318	25.327	0.424	0.531
QS64	1	0.894	0.281	8.243	25.152	0.424	0.567
QS66	18	1.481	0.264	8.153	24.991	0.426	0.540
M94	21	7.257	4.319	39.687	0	0	1.232
NM00	21	2.108	0.446	22.176	0	0	1.248

Table 2. Expanded tabulation of data at 10 kbar, 800°C, at 0.015, 0.040 and 0.43 X_{KCl} used in determining uncertainty (see text and Figures 3-6). Average values for X_{H2O}, a_{H2O}, X_{KCl} and 10^3*X_{SiO2} and m_{SiO2} are shown in Table 1.

FIGURES

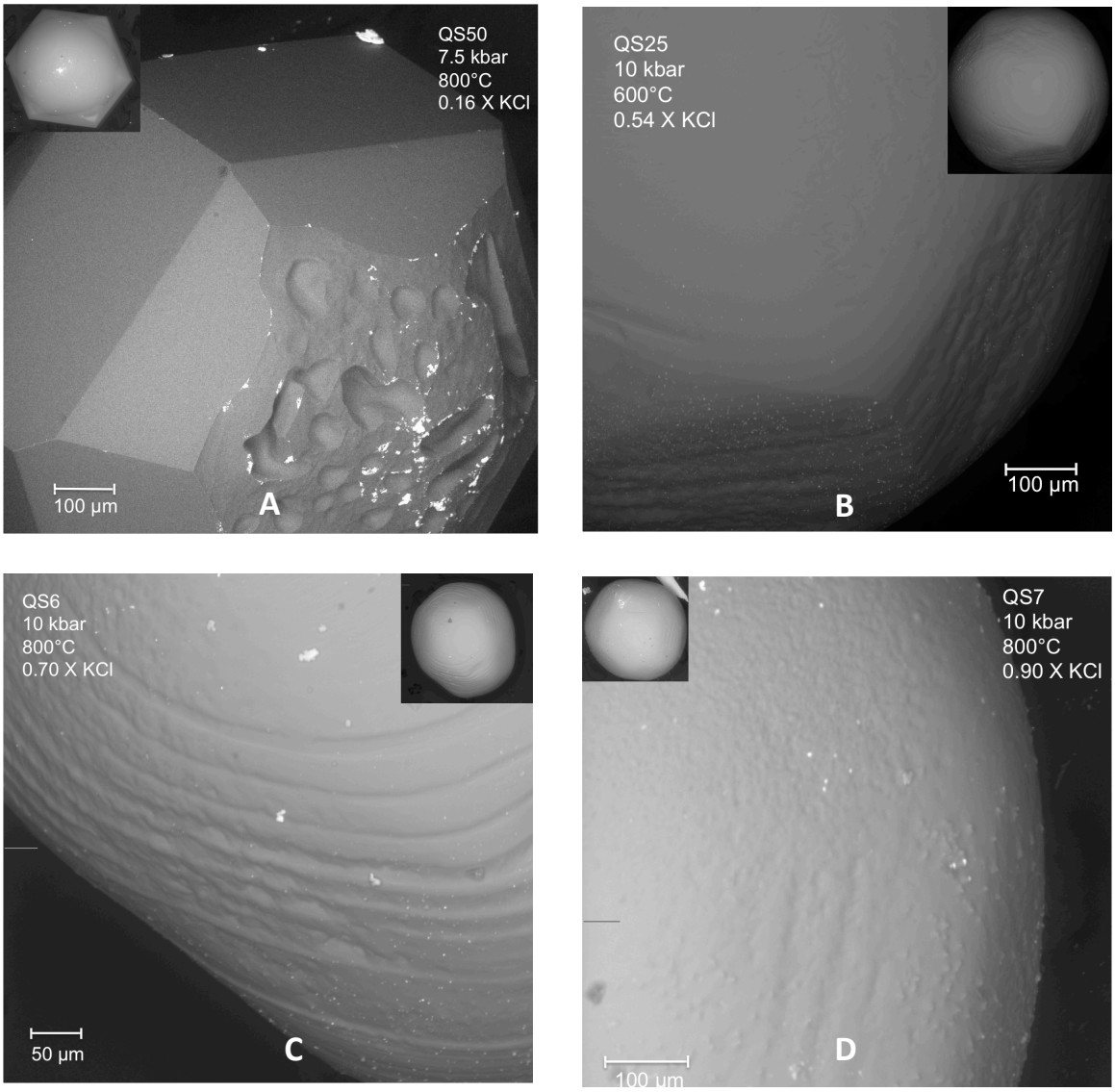

Figure 1. Dissolution textures of post-run quartz crystals from (A) intense to (B, C) intermediate to (D) weak. P, T and X_{KCl} conditions are indicated with X_{KCl} being the primary control of crystal modification. Textures are correlated with solubility measurements (Figs. 7-12).

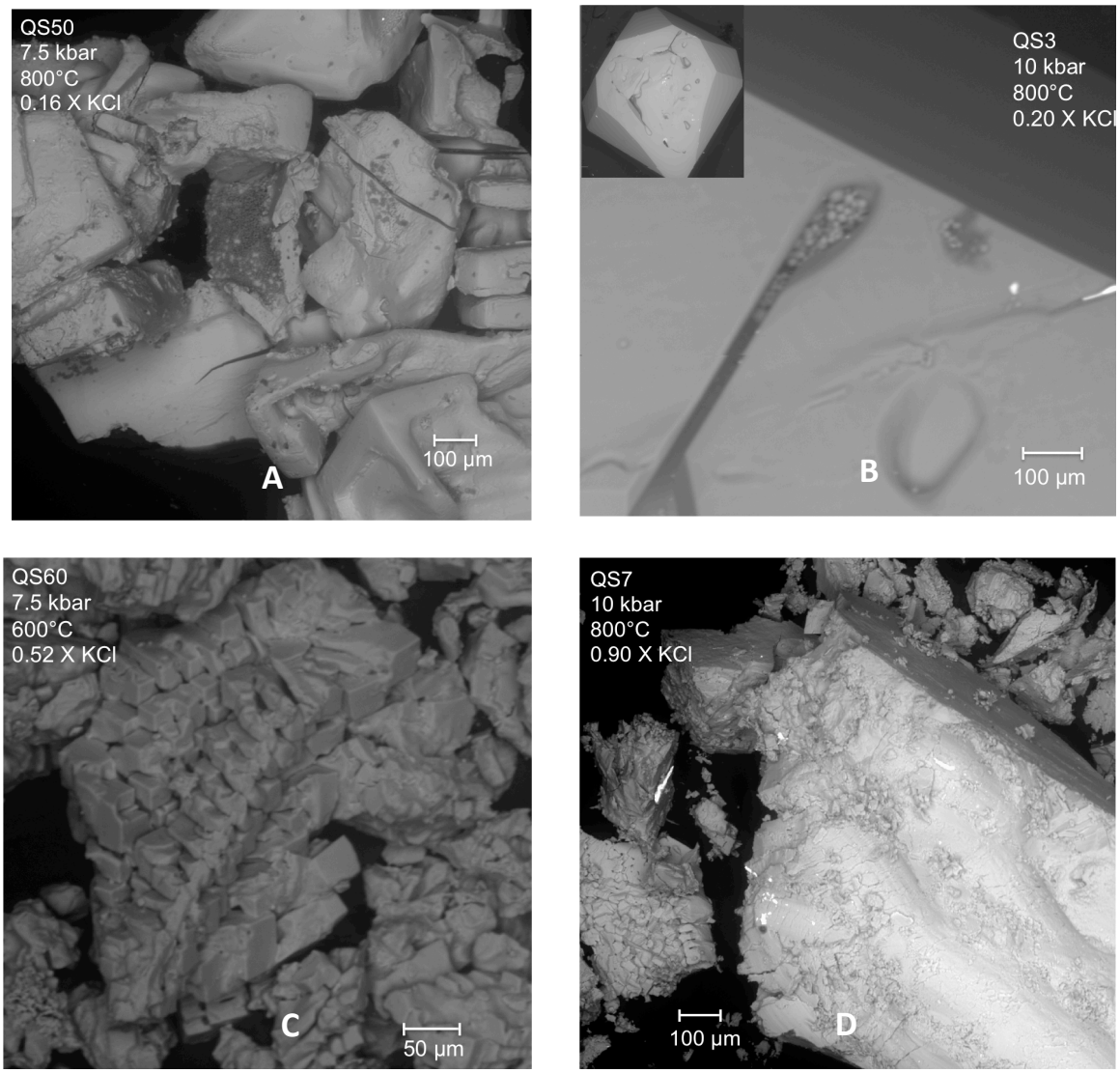

Figure 2. Quench products (i.e., contents of Pt capsule recovered post run) consisting of (A) KCl precipitates and (B) colloidal silica from dilute solutions; and (C, D) sylvite phenocrysts in saturated solutions.

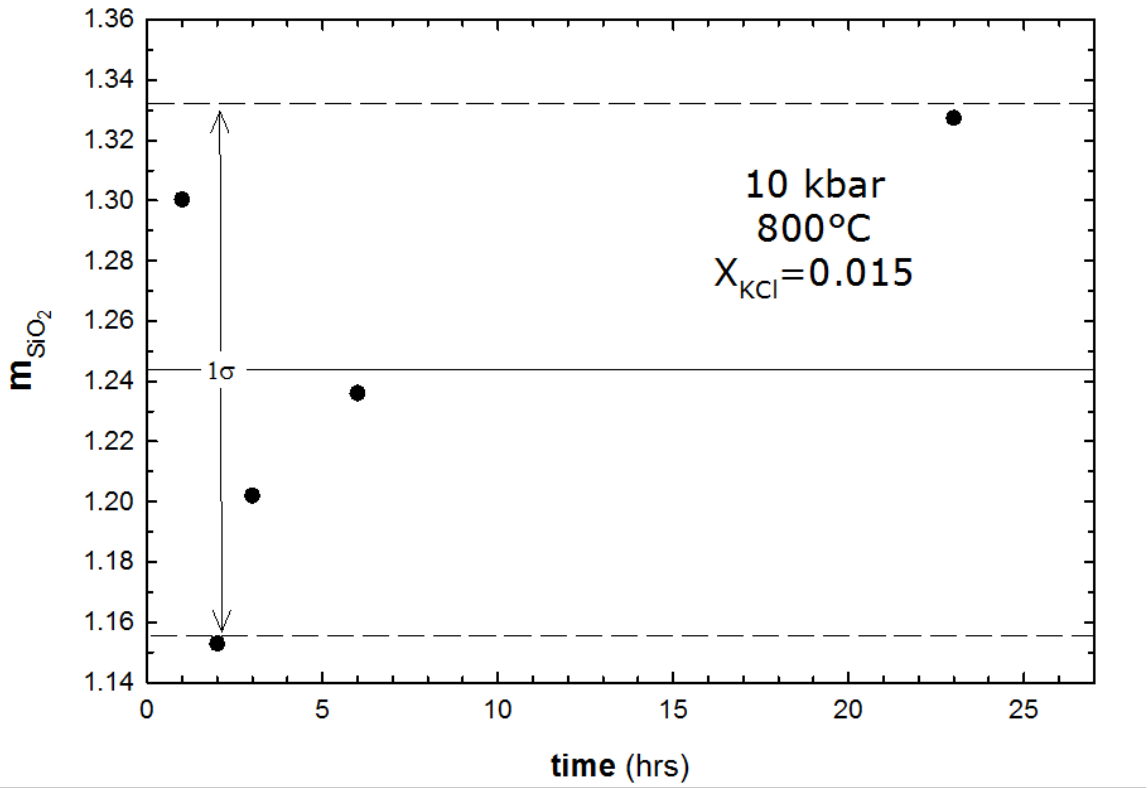

Figure 3. Solubility as a function of time at 10 kbar and 800°C, and 0.015 X_{KCl} up to 23 hours. No systematic time-dependent variation of solubility is found within the given time range. However, the standard deviation shows X_{KCl} dependence when compared with Figs. 4 and 5.

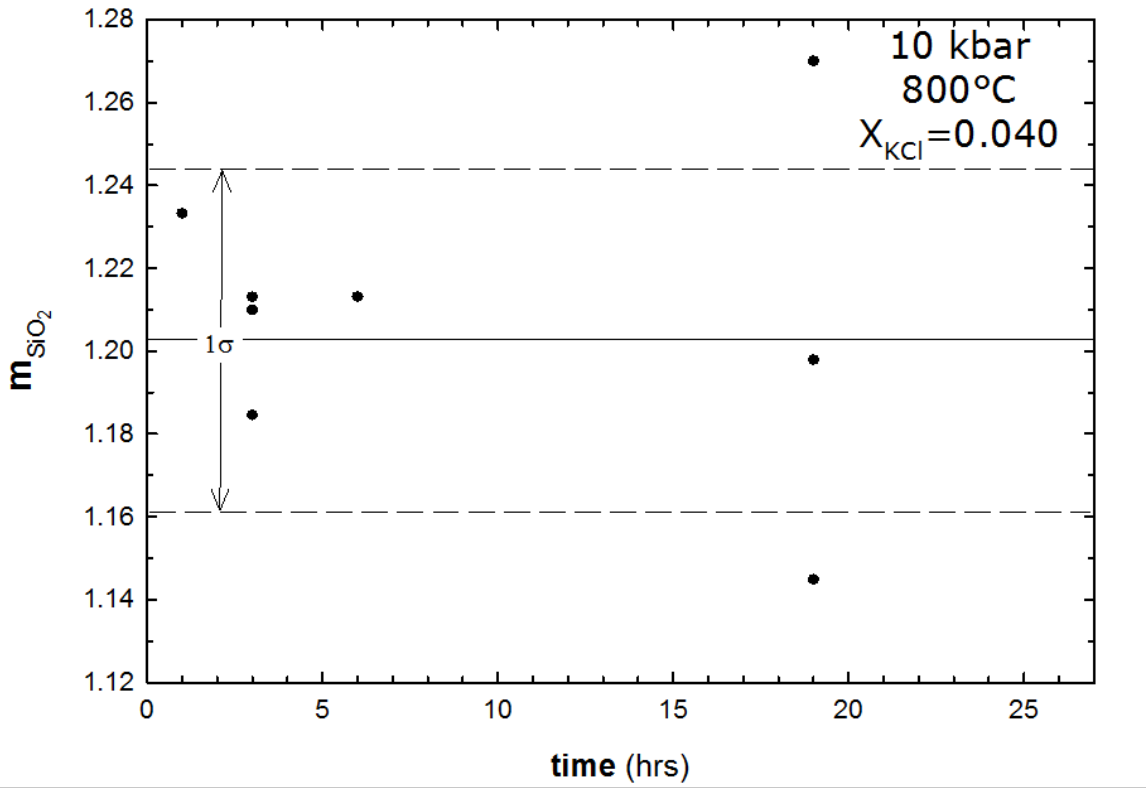

Figure 4. Solubility as a function of time at 10 kbar and 800°C, and 0.040 X_{KCl} up to 19 hours. No systematic time-dependent variation of solubility is found within the given time range. However, the standard deviation shows X_{KCl} dependence when compared with Figs. 3 and 5.

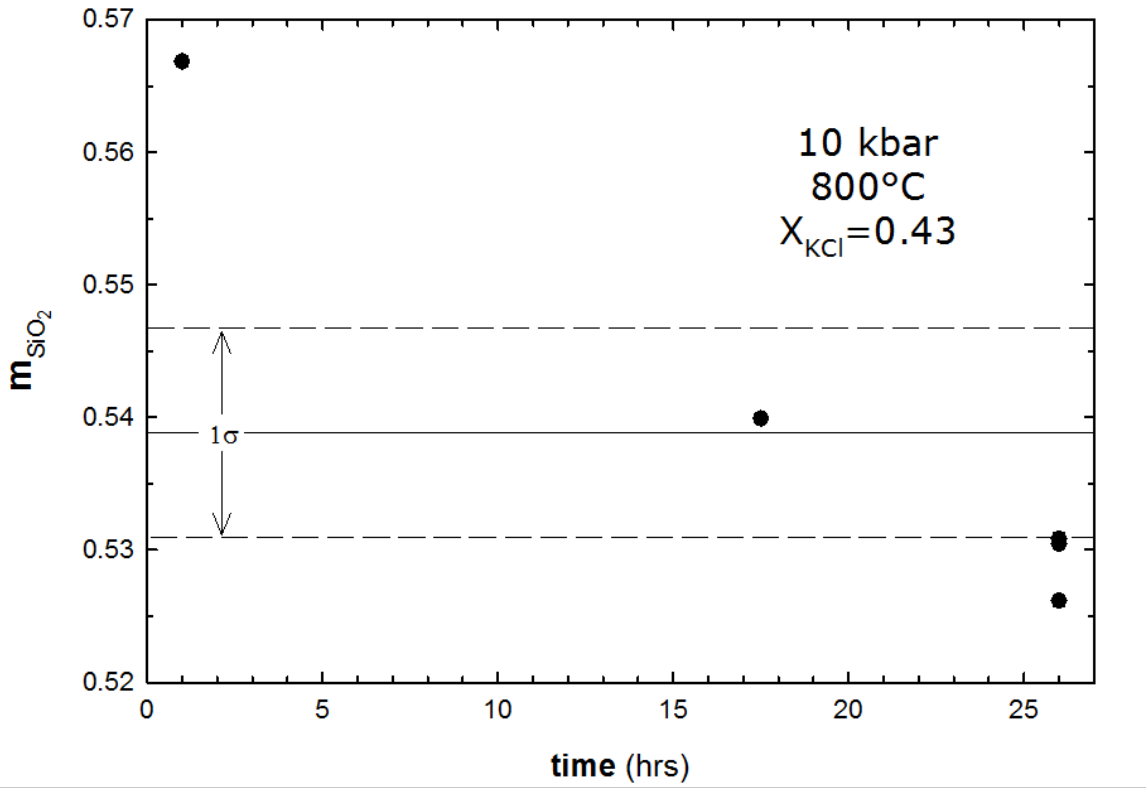

Figure 5. Solubility as a function of time at 10 kbar and 800°C, and 0.43 X_{KCl} up to 26 hours. No systematic time-dependent variation of solubility is found within the given time range. However, the standard deviation shows X_{KCl} dependence when compared with Figs. 3 and 4.

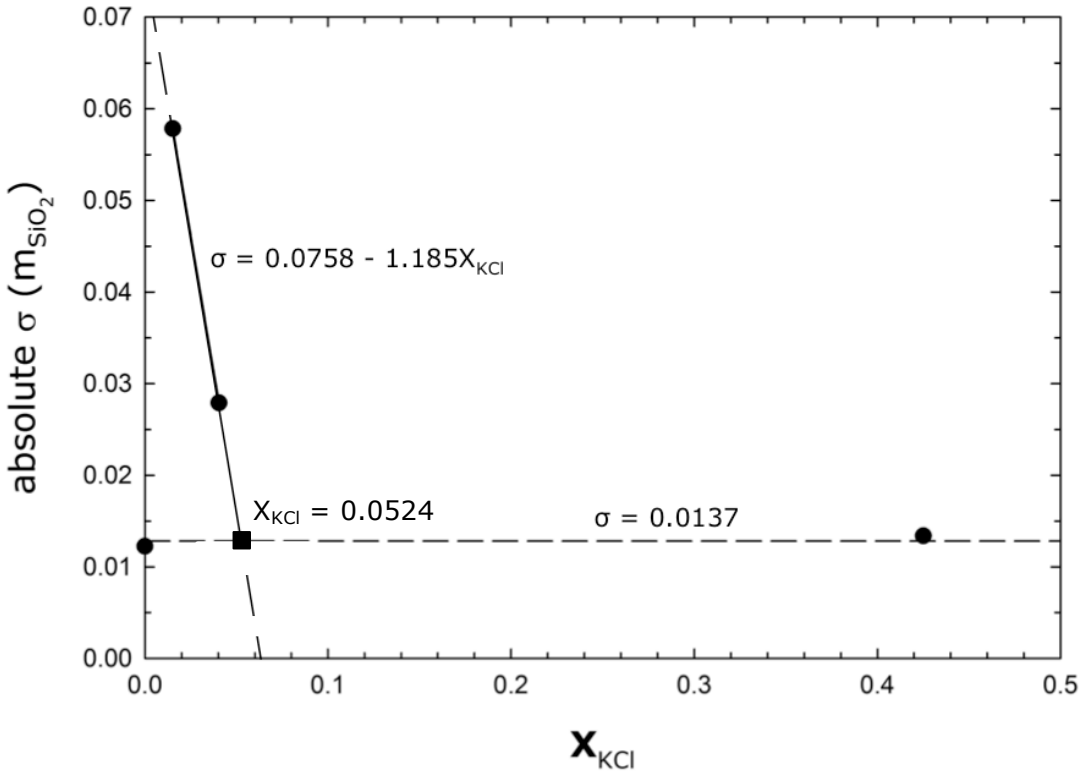

Figure 6. Plots of Equations 1 and 2; standard deviation of solubility as a function of X_{KCl}. Short dashed line represents the range for σ = 0.0137 except at $0.015 < X_{KCl} \leq 0.0524$ where the solid line function applies. Long dashed lines are σ extrapolations and are not applied.

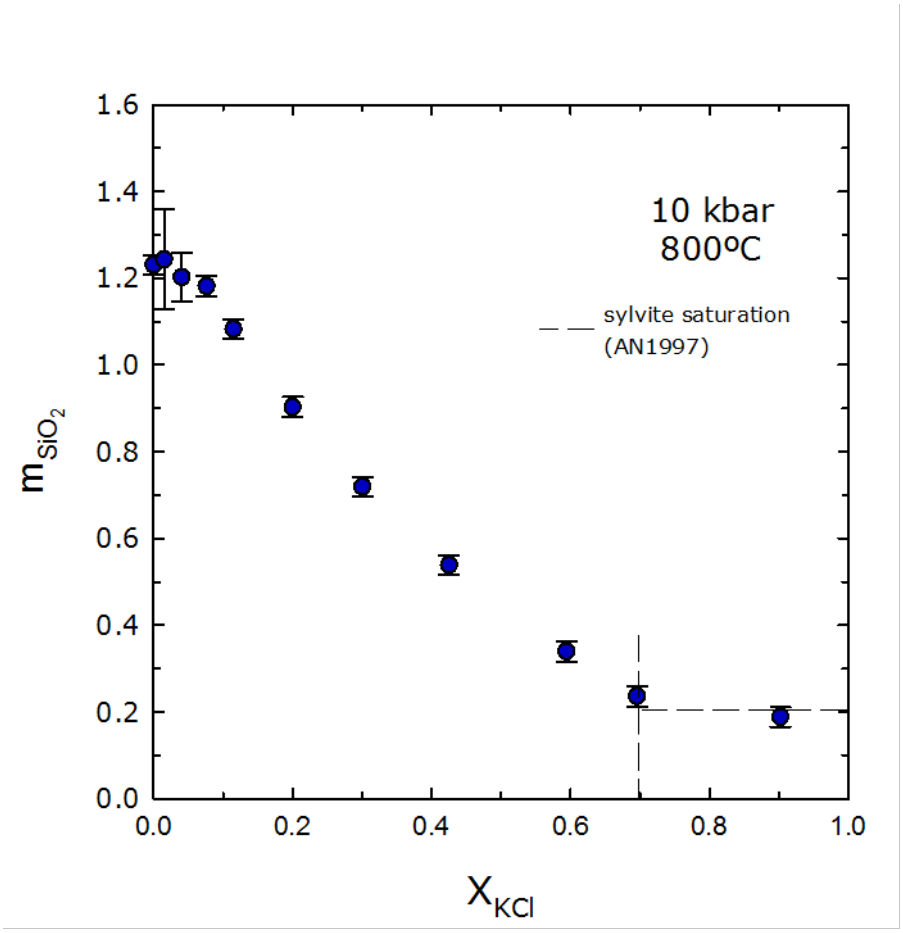

Figure 7. Silica solubility in molality (mol SiO_2/kg H_2O) at 10 kbar and 800°C showing monotonic decrease. Sylvite saturation ($X_{KCl\ sat}$) is predicted by Aranovich et al. (1997) at X_{KCl} = 0.70 and is confirmed by solubility measurements and quench product textures of this study.

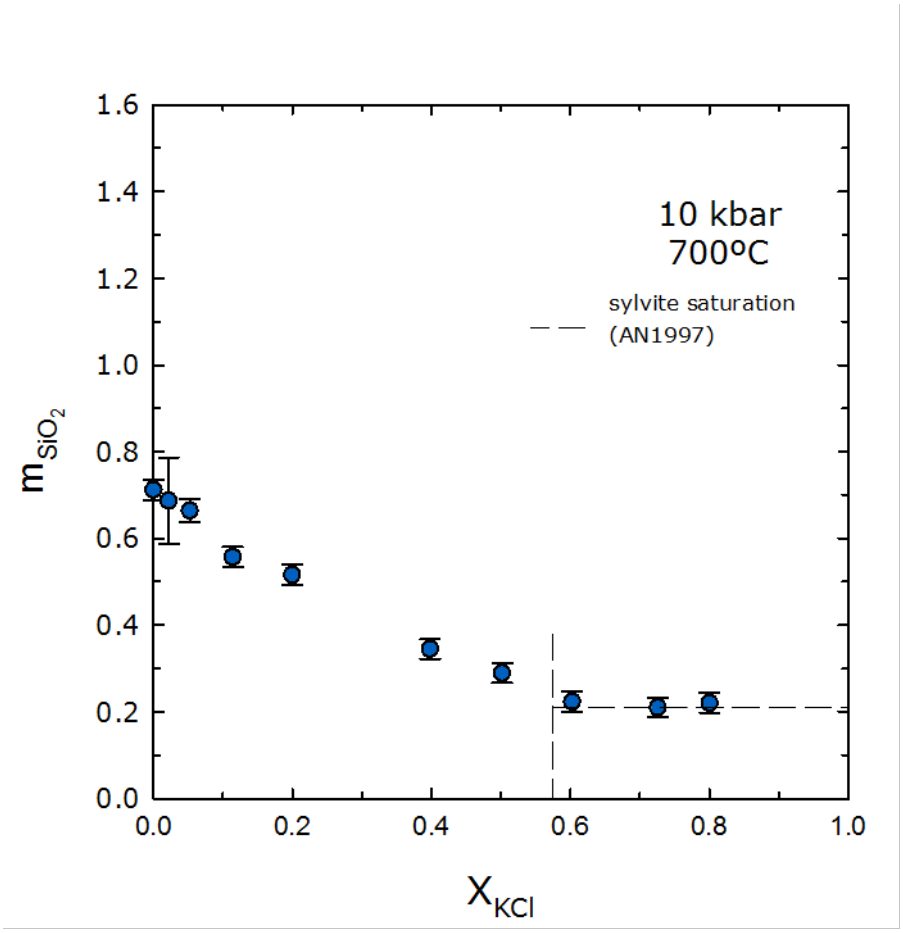

Figure 8. Silica solubility in molality (mol SiO_2/kg H_2O) at 10 kbar and 700°C showing monotonic decrease. Sylvite saturation ($X_{KCl\ sat}$) is predicted by Aranovich et al. (1997) at X_{KCl} = 0.57 and is confirmed by solubility measurements and quench product textures of this study.

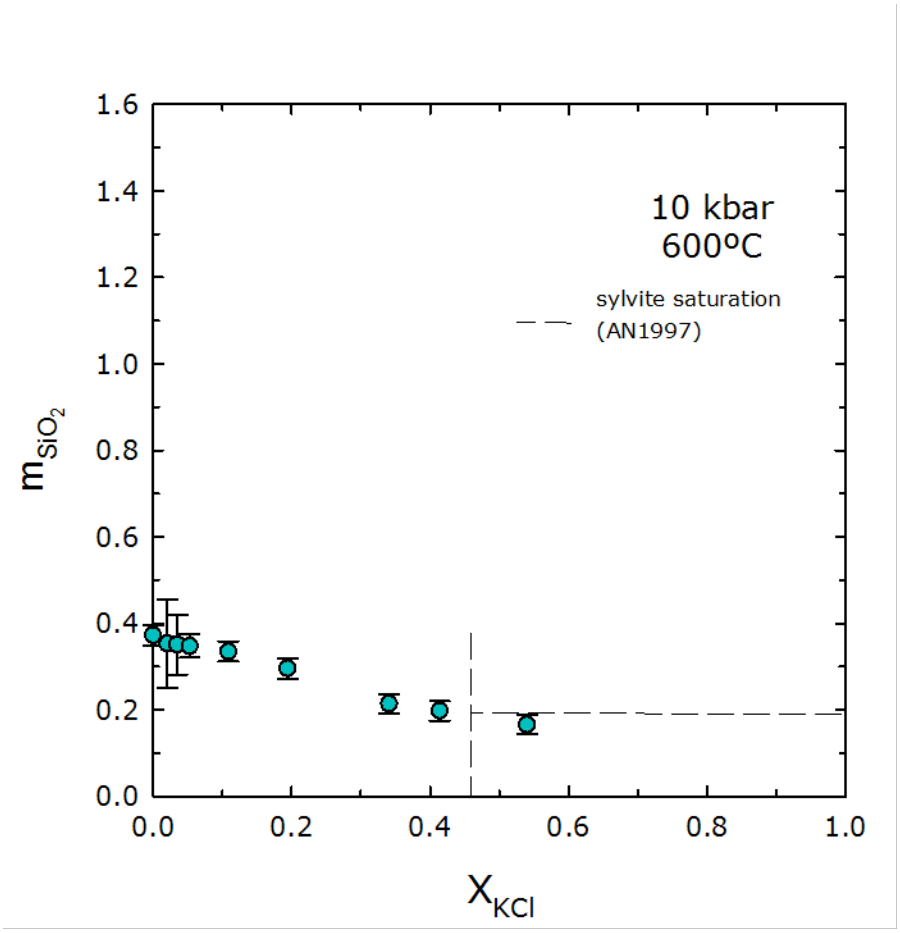

Figure 9. Silica solubility in molality (mol SiO_2/kg H_2O) at 10 kbar and 600°C showing monotonic decrease. Sylvite saturation ($X_{KCl\ sat}$) is predicted by Aranovich et al. (1997) at X_{KCl} = 0.46 and is confirmed by solubility measurements and quench product textures of this study.

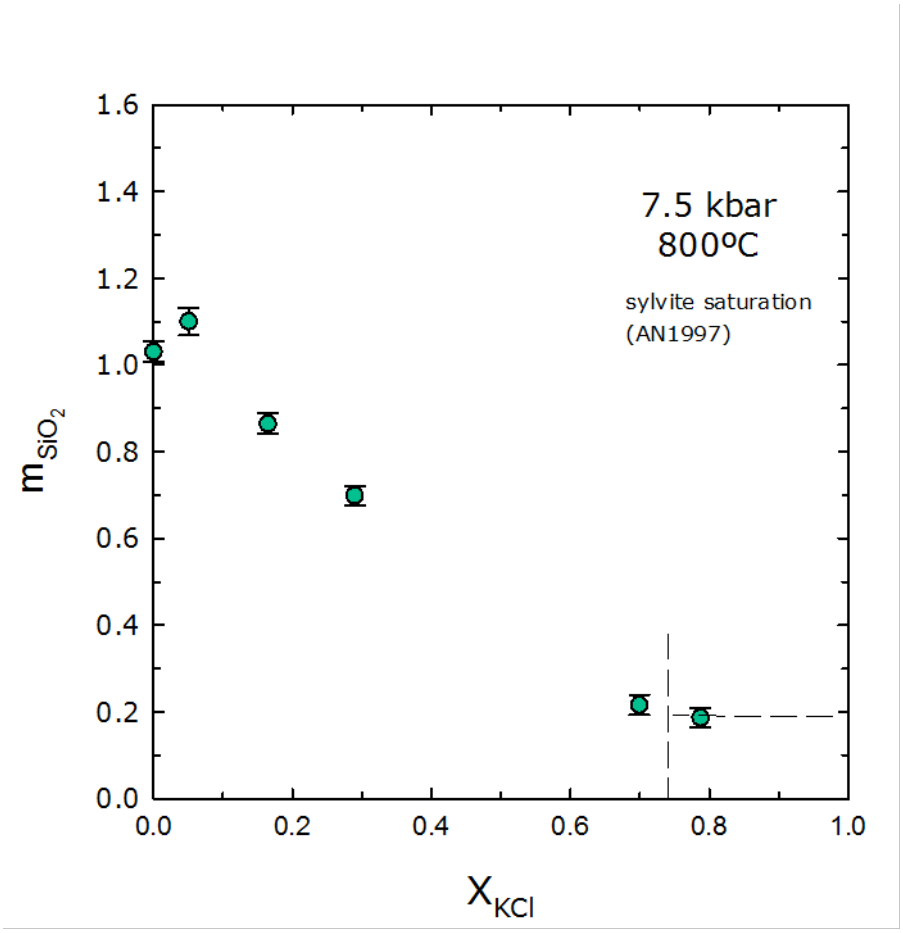

Figure 10. Silica solubility in molality (mol SiO_2/kg H_2O) at 7.5 kbar and 800°C showing very slight salting in prior to monotonic decrease. Sylvite saturation ($X_{KCl\ sat}$) is predicted by Aranovich et al. (1997) at $X_{KCl} = 0.74$ and is confirmed by solubility measurements and quench product textures of this study.

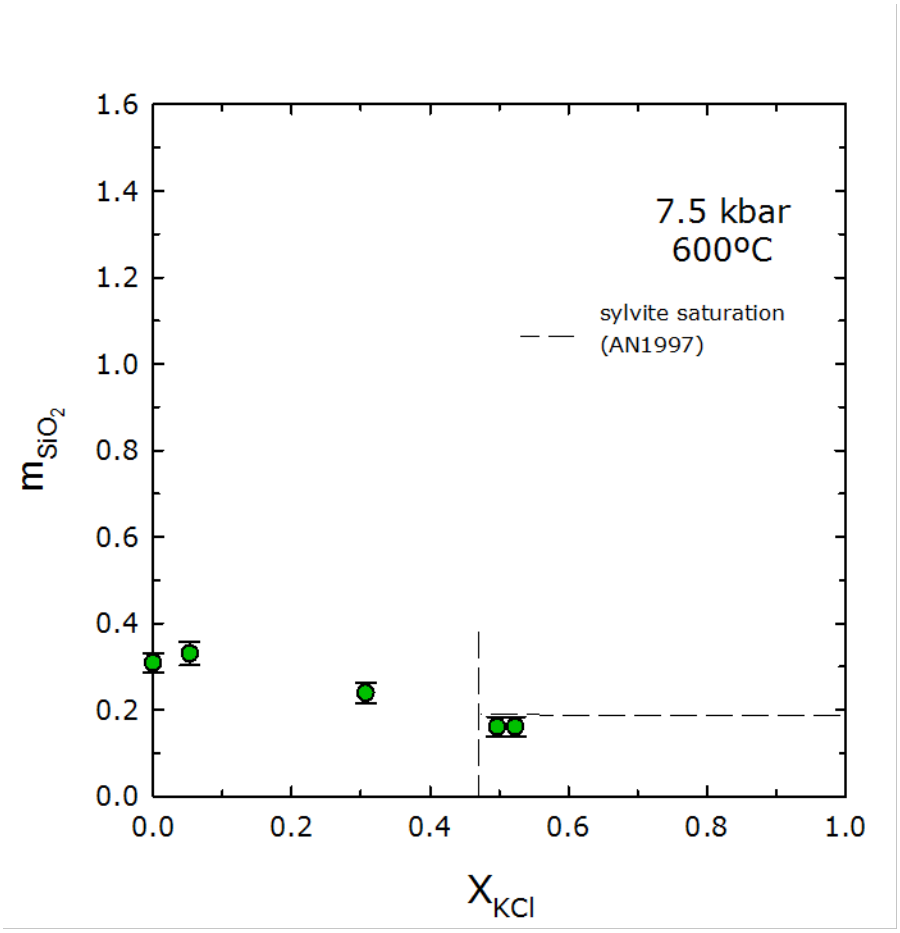

Figure 11. Silica solubility in molality (mol SiO_2/kg H_2O) at 7.5 kbar and 600°C showing very slight salting in prior to monotonic decrease. Sylvite saturation ($X_{KCl\ sat}$) is predicted by Aranovich et al. (1997) at $X_{KCl} = 0.47$ and is confirmed by solubility measurements and quench product textures of this study.

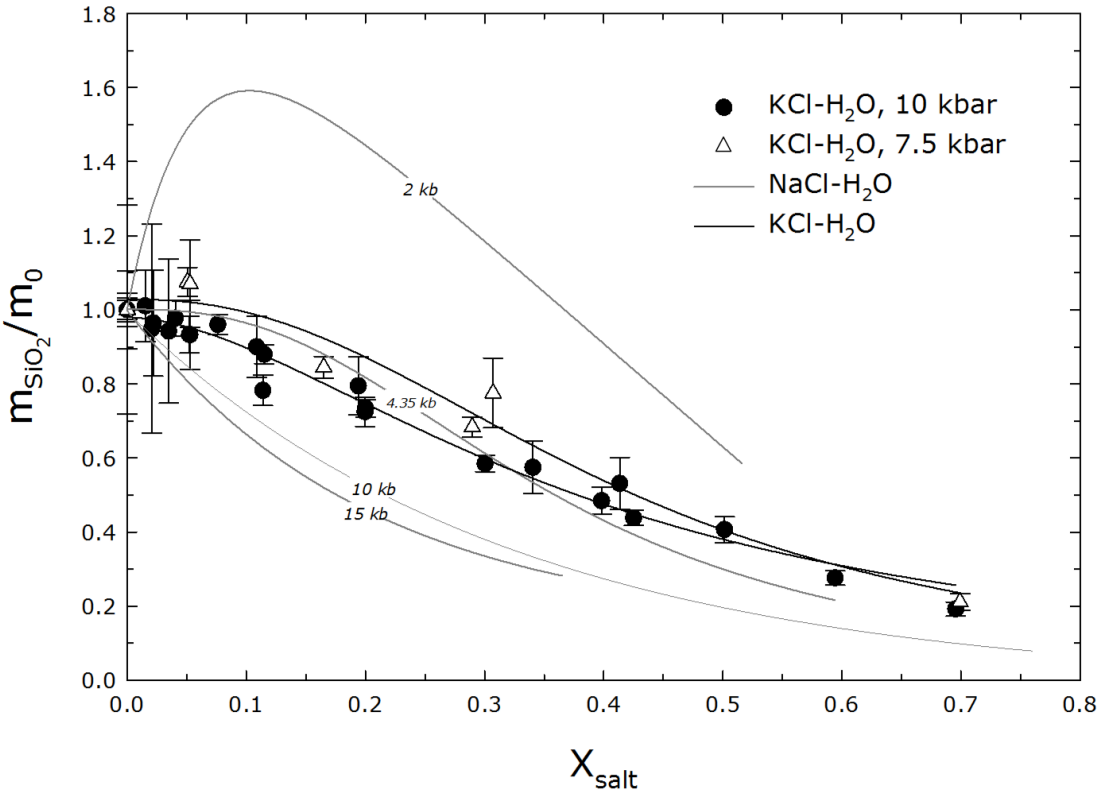

Figure 12. Relative molality, i.e., molality normalized against molality in pure H_2O, in KCl-H_2O solutions is temperature dependent, similar to that in NaCl-H_2O solutions. However, KCl-H_2O solutions dissolve more silica at the same X_{KCl}. Very slight salting in (see text for explanation) is present 7.5 kbar but absent in 10 kbar. Data at $X_{KCl} > X_{KCl\ sat}$ are disregarded since they represent $a_{H_2O} = 0$. NaCl-H_2O data are from Newton and Manning (2010).

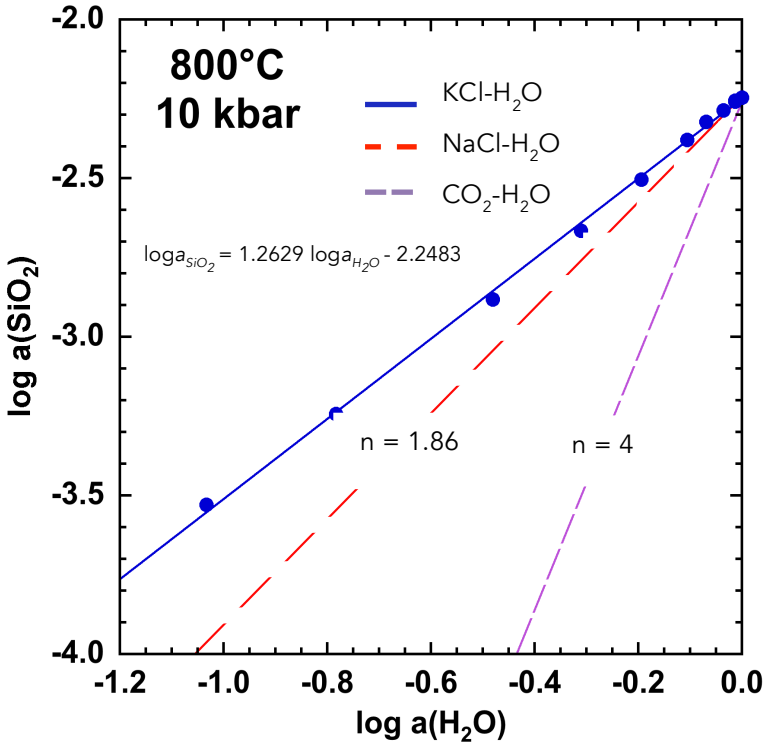

Figure 13. Slopes from linear fits to data correspond to *n*, the total hydration number; the lower *n* and higher solubility of quartz in KCl–H_2O at a given H_2O activity implies solubility enhancement (Newton and Manning, 2010).

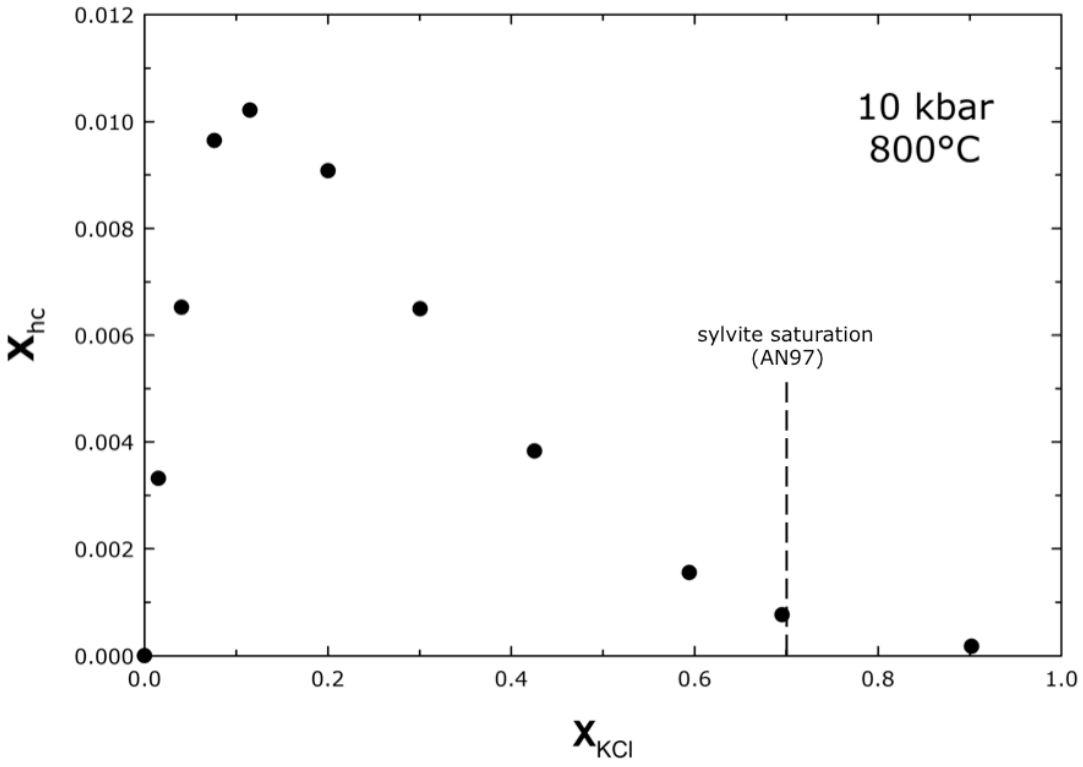

Figure 14. Concentration of silica in proposed hybrid complex, X_{hc}, as a function of X_{KCl} at 10 kbar and 800°C. Silica solubility enhancement is attributed to the formation of hybrid complexes, peaking at about X_{KCl} =0.12. Sylvite saturation is from Aranovich et al. (1997).

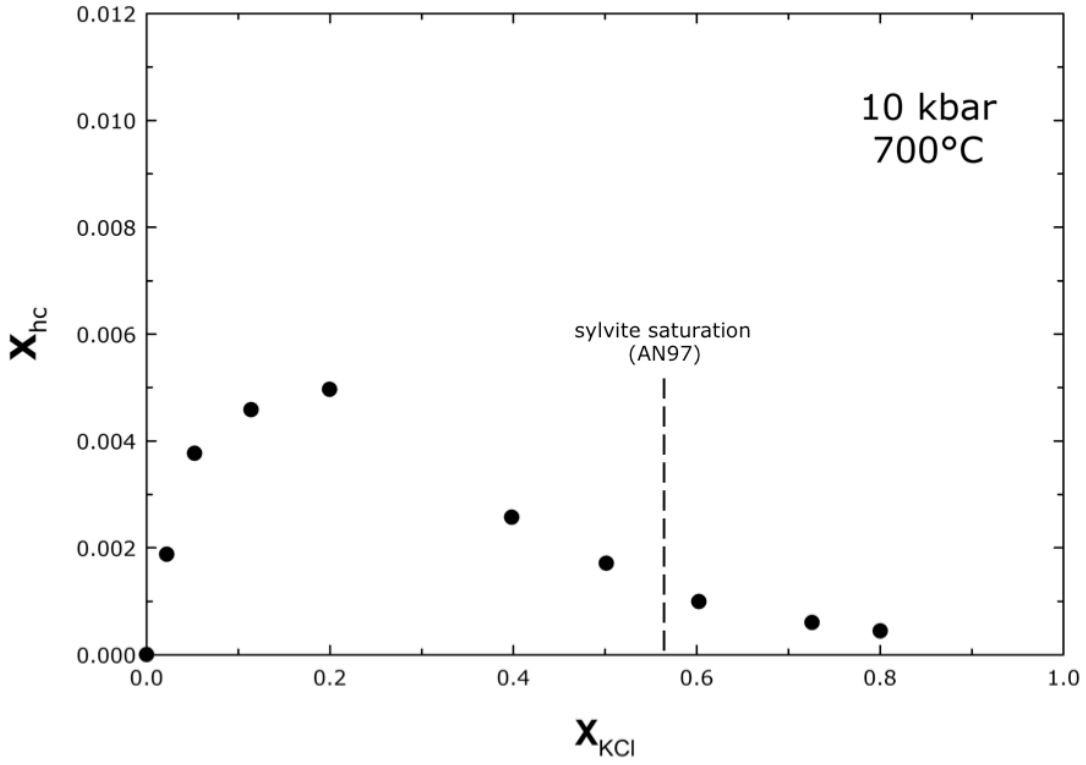

Figure 15. Concentration of silica in proposed hybrid complex, X_{hc}, as a function of X_{KCl} at 10 kbar and 700°C. Sylvite saturation is from Aranovich et al. (1997).

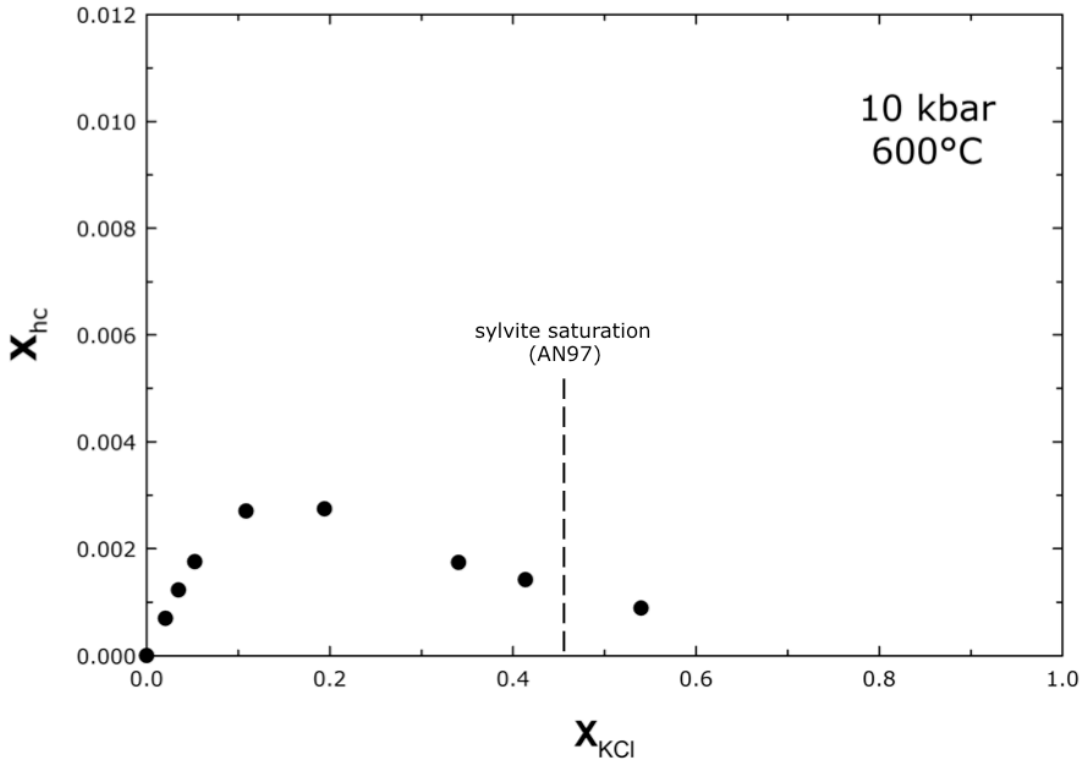

Figure 16. Concentration of silica in proposed hybrid complex, X_{hc}, as a function of X_{KCl} at 10 kbar and 600°C. Sylvite saturation is from Aranovich et al. (1997).

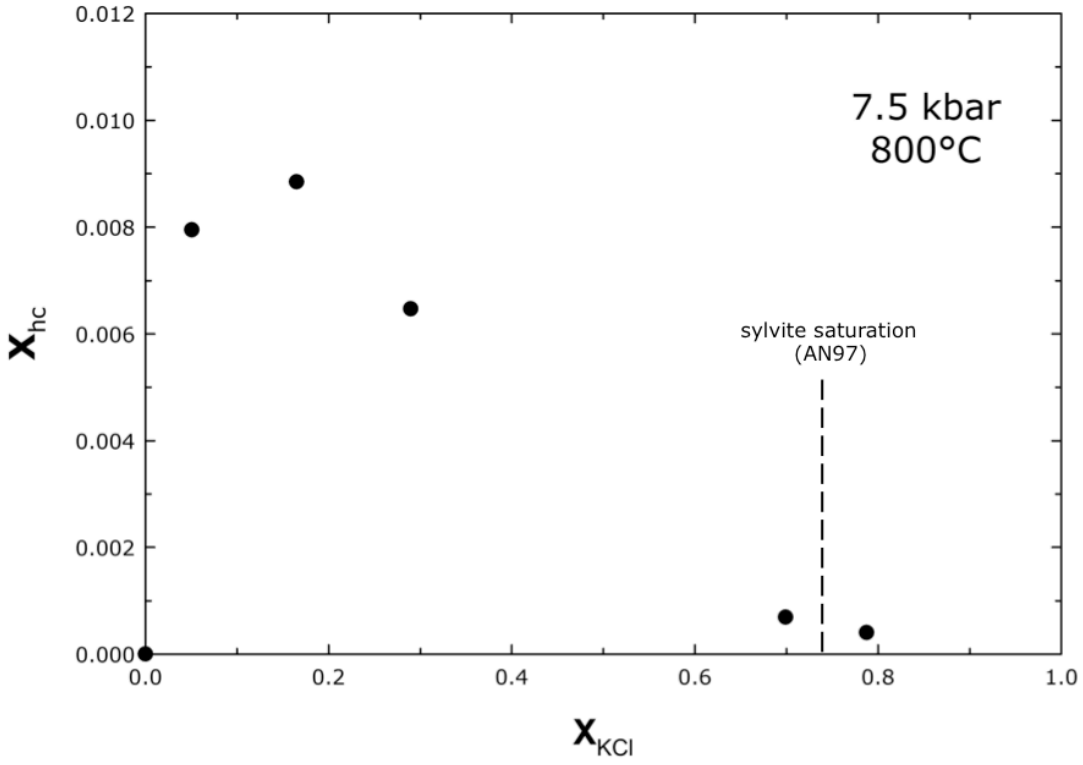

Figure 17. Concentration of silica in proposed hybrid complex, X_{hc}, as a function of X_{KCl} at 7.5 kbar and 800°C. Sylvite saturation is from Aranovich et al. (1997).

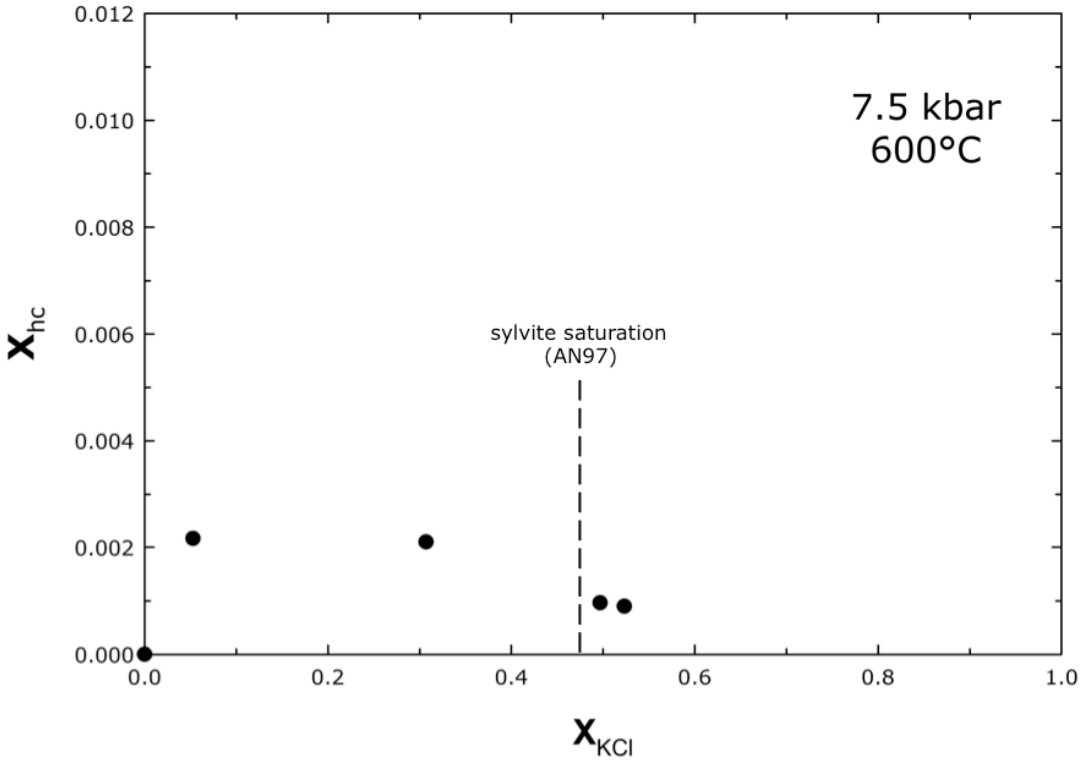

Figure 18. Concentration of silica in proposed hybrid complex, X_{hc}, as a function of X_{KCl} at 7.5 kbar and 600°C. Sylvite saturation is from Aranovich et al. (1997).

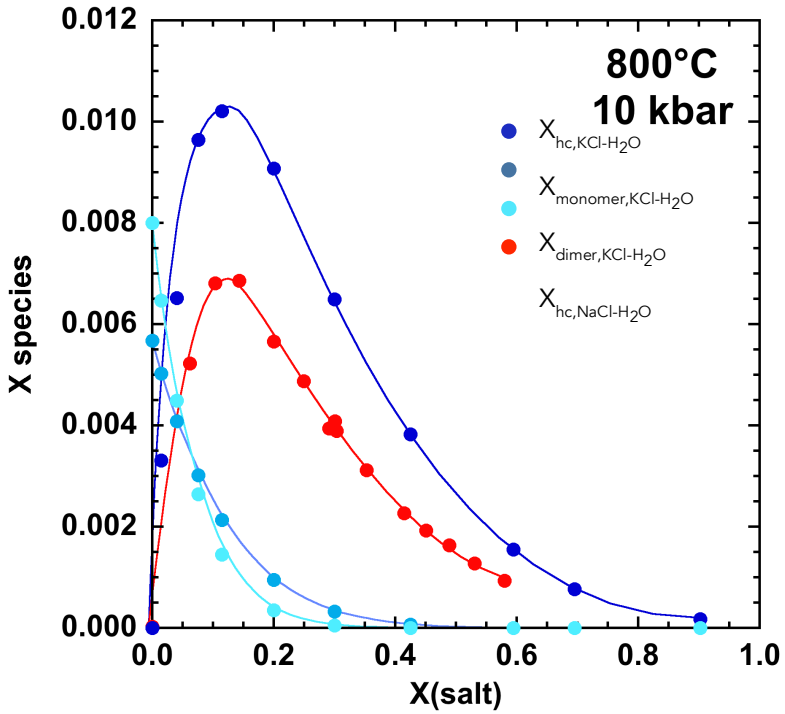

Figure 19. Mole fraction of silica in hybrid complex, monomer and dimer in KCl-H_2O solutions from this study; and that of silica in hybrid complex in NaCl-H_2O solutions from Newton and Manning (2010). Plot shows greater abundance of solubility-enhancing complexes in KCl-H_2O solutions at 10 kbar and 800°C.

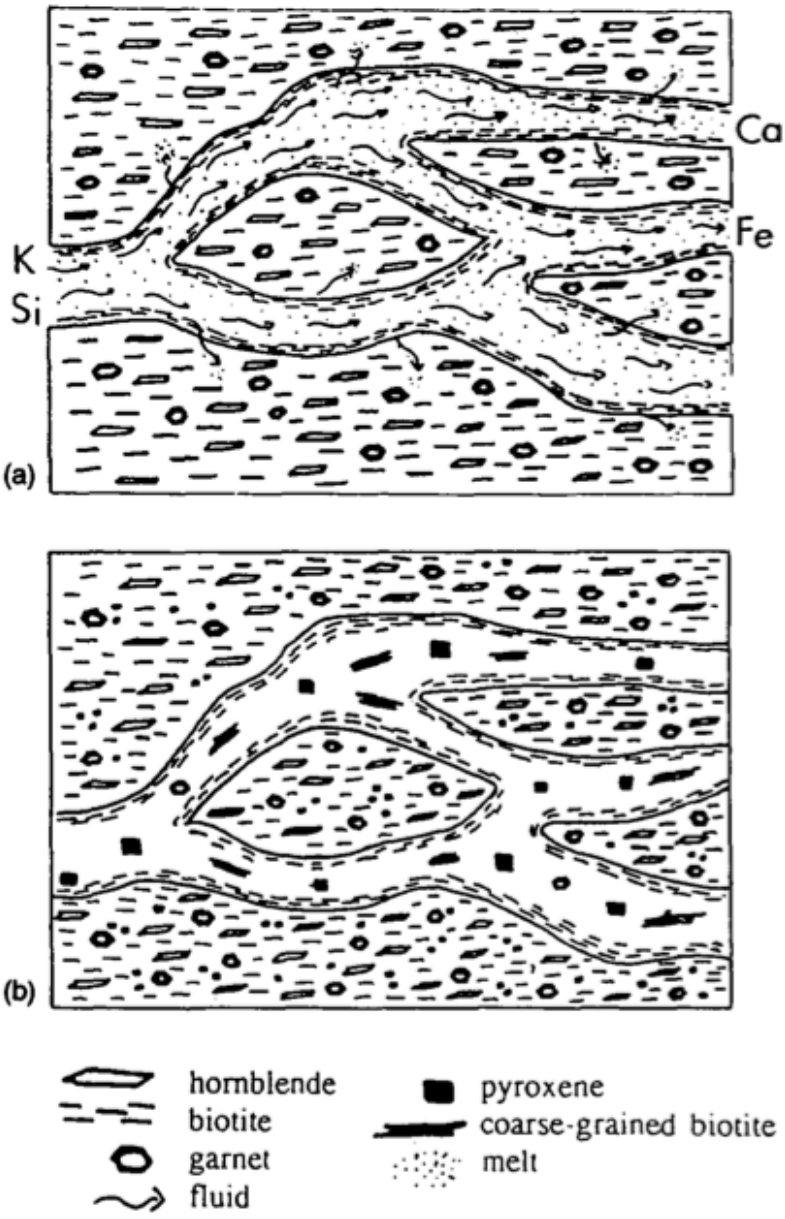

Figure 20. The open-system homogeneous melting model from Hansen and Stuk (1993). (a) During the peak of metamorphism, fluid permeates through channels adding Si and K while removing Ca and possibly Fe. Extensive melting occurs along these channels. (b) The melt crystallizes and form coarse-grained leucocratic veins.

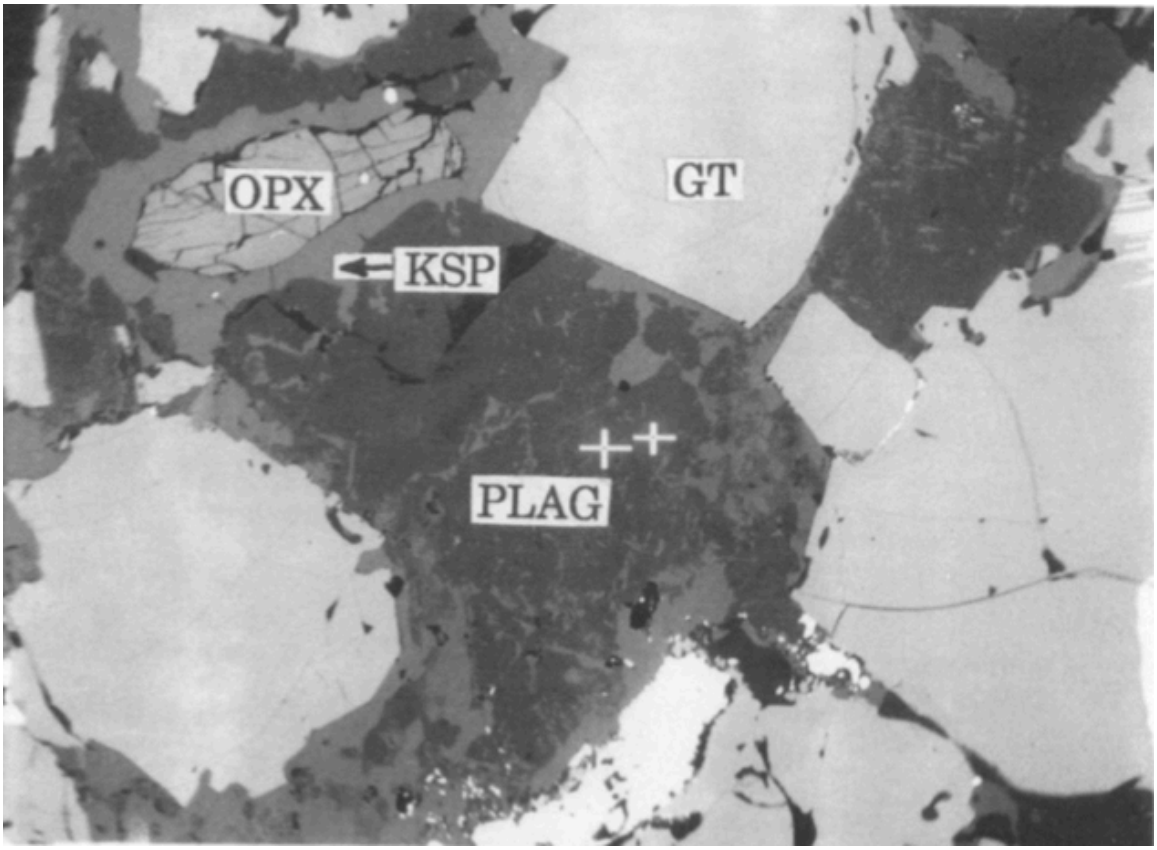

Figure 21. BSE image of a charnockite from Shevaroy Hills, south India. Gt = garnet, Opx = orthopyroxene, Plag = plagioclase, Ksp = K-feldspar. High-Ba Ksp appear as replacement of plagioclase as well as grain-boundary lining of Opx and Gt. The fluid must have low H_2O activity for compatibility of orthopyroxene and K-feldspar (Hansen et al., 1995).

REFERENCES

Anderson G.M. and Burnham C.W. (1965). Solubility of quartz in supercritical water. *American Journal of Science*, 263, 494–511.

Anderson, G.M. and Burnham, C.W. (1967). Reactions of quartz and corundum with aqueous chloride and hydroxide solutions at high temperatures and pressures. *American Journal of Science*, 265, 12–27.

Antignano, A. (2008). Apatite and rutile solubility in water–sodium chloride and silicate-bearing fluids at high temperatures and pressures: Implications for metamorphic fluids. Unpublished Ph.D. Thesis, University of California, Los Angeles, 94 pp.

Aranovich, L. Y. and Newton, R. C. (1996). H_2O activity in concentrated NaCl solutions at high pressures and temperatures measured by the brucite-periclase equilibrium. *Contributions to Mineralogy and Petrology*, 125(2-3), 200–212.

Aranovich, L. Y. and Newton, R. C. (1997). H_2O activity in concentrated KCl and KCl-NaCl solutions at high temperatures and pressures measured by the brucite-periclase equilibrium. *Contributions to Mineralogy and Petrology*, 127(3), 261–271.

Aranovich, L.Y., Newton, R.C., and Manning, C.E. (2013). Brine-assisted anatexis: exper-imental melting in the system haplogranite–H2O–NaCl–KCl at deep-crustal conditions. *Earth Planetary Science Letters*, 374, 111–120.

Aranovich, L. Y., Makhluf, A. R., Manning, C. E., and Newton, R. C. (2014). Dehydration melting and the relationship between granites and granulites. *Precambrian Research*, *253*, 26-37.

Ayers, J.e., Brenan, J.M., Watson, E.B., Wark, D.A., and Minarik, W.B. (1992) A new capsule technique for hydrothermal experiments using the piston-cylinder apparatus. *American Mineralogist*, 77, 1080-1086.

Bachmann, O. and Bergantz, G.W. (2006). Gas percolation in upper-crustal silicic crystal mushes as a mechanism for upward heat advection and rejuvenation of near- solidus magma bodies. *Journal of Volcanology Geothermal Research*, Res. 149, 85–102.

Barker, D.S. (1996). Consequences of recycled carbon in carbonatites. *Canadian Mineralogist*, 34, 373–387.

Bebout, G.E and Barton M.D. (1993) Metasomatism during subduction – products and possible paths in the Catalina schist, California. *Chemical Geology*, 108, 61–92.

Bohlen, R. (1984) Equilibria for precise pressure calibration and a frictionless furnace assembly for the piston-cylinder apparatus. *Neues Jahrbuch für Mineralogie, Monatsheft,* 9, 404-412.

Bohlen, S.R., Boettcher, A. L.; Wall, V. J. and Clemens, J. D. (1983). Stability of phlogopite-quartz and sanidine-quartz: a model for melting in the lower crust: *Contributions to Mineralogy and Petrology*, 83, 270-277.

Burnham C.W., Holloway J.R., and Davis N.F. (1969). Thermodynamic properties of water to 1,000°C and 10,000 bars. *Geological Society of America Special Paper* 132.

Caciagli, N. C. and Manning, C. E. (2003). The solubility of calcite in water at 6–16 kbar and 500–800°C. *Contributions to Mineralogy and Petrology*, 146(3), 275-285.

Coolen, J. M. (1980). Chemical petrology of the Furua Granulite Complex, southern Tanzania: *Free University Amsterdam Geological Paper*, Ser. 1, n. 13-1980, 258.

Crerar D.A. and Anderson G.M. (1971) Solubility and solvation reactions of quartz in dilute hydrothermal solutions. *Chemical Geology*, 8, 107–22.

Cruz, M. F. and Manning, C. E. (2015). Experimental determination of quartz solubility and melting in the system SiO_2–H_2O–NaCl at 15–20 kbar and 900–1100°C: implications for silica polymerization and the formation of supercritical fluids. *Contributions to Mineralogy and Petrology*, *170*(4), 1-17.

Evans, K. (2007). Quartz solubility in salt‐bearing solutions at pressures to 1 GPa and temperatures to 900° C. *Geofluids*, *7*(4), 451-467.

Ganguly, J., Singh, R.N. and Ramana, D.V. (1995). Thermal perturbation during charnockitization and granulite facies metamorphism in southern India. *Journal of Metamorphic Geology*. 13, 419–430.

Hansen, E. and Stuk, M. (1993). Orthopyroxene‐bearing, mafic migmatites at Cone Peak, California: evidence for the formation of migmatitic granulites by anatexis in an open system. *Journal of Metamorphic Geology*, *11*(2), 291-307.

Hansen, E. C., Newton, R. C., Janardhar, A. S., and Lindenberg, S. (1995). Differentiation of late Archean crust in the eastern Dharwar craton, Krishnagiri-Salem area, south India. *The Journal of Geology*, 629-651.

Johnson, E.L. (1991). Experimentally determined limits for H_2O–CO_2 –NaCl immisci- bility in granulites. *Geology*, 19, 925–928.

Kennedy, G. (1950). A portion of the system silica-water. *Economic Geology*, 45, 629–53.

Lund M.D., Piazolo S., and Harley, S.L. (2006). Ultrahigh temperature deformation microstructures in felsic granulites of the Napier complex, Antarctica. *Tectonophysics*, 427, 133–151.

Manning C.E. (1994). The solubility of quartz in H2O in the lower crust and upper mantle. *Geochimica et Cosmochimica Acta*, 58, 4831–9.

Manning C. E. and Boettcher(1994). Rapid-quench hydrothermal experiments at mantle pressures and temperatures. *American Mineralogist*, 79, 1153-1158.

Newton R.C. and Manning C.E. (2000). Quartz solubility in H2O and H2O-CO2 solutions at deep crust-upper mantle pressures and temperatures: 2–15 kbar and 500–900C. *Geochimica et Cosmochimica Acta*, 64, 2993–3005.

Newton, R. C. and Manning, C. E. (2003). Activity coefficient and polymerization of aqueous silica at 800°C, 12 kbar, from solubility measurements on SiO_2-buffering mineral assemblages. *Contributions to Mineralogy and Petrology*, *146*(2), 135-143.

Newton, R. C. and Manning, C. E. (2006). Solubilities of corundum, wollastonite and quartz in H_2O–NaCl solutions at 800°C and 10 kbar: Interaction of simple minerals with brines at high pressure and temperature. *Geochimica et Cosmochimica Acta*, *70*(22), 5571-5582.

Newton, R. C. and Manning, C. E. (2009). Letter. Hydration state and activity of aqueous silica in H_2O-CO_2 fluids at high pressure and temperature. *American Mineralogist*, *94*(8-9), 1287-1290.

Newton, R. C. and Manning, C.E. (2015). Evidence for SiO_2-NaCl complexing in H_2O-NaCl solutions at high pressure and temperature. *Geofluids*.

Novgorodov, P. G. (1975). Quartz solubility in H_2MO2 mixtures at 700°C and pressures of 3 and 5 kbar. *Geokhimica*, no. 10, 1484-1489.

Olsen, S. N. (1985). Mass balance in migmatites. In: *Migmatites* (ed. Ashworth, 1. R.), pp. 145-179. Blackie. Glasgow.

Pattison, D. R. M. and Newton, R. C. (1989). Reversed experimental calibration of the garnet-clinopyroxene Fe-Mg exchange thermometer. *Contributions to Mineralogy and Petrology,* 101, 87-103.

Perchuk, L. L. and Gerya, T. V. (1992). The fluid regime of metamorphism and the charnockite reaction in granulites: a review. *International Geology Review*, *34*(1), 1-58.

Perchuk, L. L. and Gerya, T. V. (1993). Fluid control of charnockitization. *Chemical Geology*, *108*(1), 175-186.

Powell, R. (1983). Processes in granulite facies metamorphism. In: *Migmatites, Melting and Metamorphism* (eds. Atherton, M. P. & Gribble, C. D.), pp. 127-139. Shiva, Nantwich.

Renard F., Gratier J.P. and Jamtveit, B. (2000). Kinetics of crack-sealing, intergranular pressure solution, and compaction around active faults. *Journal of Structural Geology*, 22, 1395–407.

Scambelluri, M. and Philippot, P. (2001). Deep fluids in subduction zones. *Lithos*, *55*(1), 213-227.

Sen, S. K. (1959). Potassium content of natural plagioclases and the origin of antiperthites. *The Journal of Geology*, 479-495.

Setchenow, M. (1892). Action de l'acide carbonique sur les solutions des sels a acides forts. In *Annales de Chimie et de Physique*, 25, 226-270.

Shettel, D. L. (1974). The Solubility of Quartz in Supercritical H_20-CO_2 Fluids. Doctoral dissertation, Pennsylvania State University.

Somerfeld R.A. (1967). Quartz solution reaction: 400°–500°C, 1000 bars. *Journal of Geophysical Research*, 72, 4253–7.

Shmulovich, K. I., Yardley, B. W. D., and Graham, C. M. (2006). Solubility of quartz in crustal fluids: experiments and general equations for salt solutions and H2O-CO2 mixtures at 400- 800 °C and 0.1-0.9 GPa. *Geofluids*, 6(2), 154–167.

Stolz, A.J. and Davies, G.R. (1989). Metasomatized lower crustal and upper mantle xeno- liths from north Queensland: chemical and isotopic evidence bearing on the composition and source of the fluid phase. *Geochimica et Cosmochimica Acta*, 53, 649–660.

Todd, C. S. and Evans, B. W. (1994). Properties of CO_2-induced dehydration of amphibolite. *Journal of Petrology*, 35, 1213-1240.

Trommsdorff, V., Skippen, G. and Ulmer, P. (1985). Halite and sylvite as solid inclusions in high-grade metamorphic rocks. *Contributions to Mineralogy and Petrology*, *89*(1), 24-29.

Ulmer P. (1983). Monticellite-clintonite-bearing assemblages at the southern border of the Adamello-Massif. *Rendiconti della Societa Italiana di Mineralogia e Petrologia*, 38, 617-628.

Vielzeuf, S. and Clemens, J. D. (1992). The fluid-absent m elting of phlogopite + quartz:

experiments and models. *American Mineralogist*, 77, 1206-1222.

Walther, J. V. and Helgeson, H. C. (1977). Calculation of the thermodynamic properties of aqueous silica and the solubility of quartz and its polymorphs at high pressures and temperatures. *American Journal of Science*, *277*(10), 1315-1351.

Walther J.V. and Orville P.M. (1983) The extraction quench technique for determination of the thermodynamic properties of solute complexes – application to quartz solubility in fluid mixtures. *American Mineralogist*, 68, 731–41.

Waters, D. J. (1988). Partial melting and the formation of granulite facies assemblages in Namaqualand, South Africa. *Journal of Metamorphic Geology,* 6, 387-400.

Weill, D. F. and Fyfe, W. S. (1964). The solubility of quartz in H_2O in the range 1000–4000 bars and 400–550° C. *Geochimica et Cosmochimica Acta*, *28*(8), 1243-1255.

Woolley, A.R., 1989. The spatial and temporal distribution of carbonatites. In: *Carbonatites: Genesis and Evolution*. Unwin Hyman, London, pp. 35–54.

Zotov, N. and Keppler, H. (2002). Silica speciation in aqueous fluids at high pressures and high temperatures. *Chemical Geology*, *184*(1), 71-82.